

Article

Structure guided design, synthesis, and biological evaluation of 2-(1H-Indol-3-yl)-1H-imidazol-4-yl(3,4,5-trimethoxyphenyl) Methanone (ABI-231) analogs targeting the colchicine binding site in tubulin

Qinghui Wang, Kinsie Arnst, Yuxi Wang, Gyanendra K Kumar,
Dejian Ma, Stephen W. White, Duane D Miller, Weimin Li, and Wei Li

J. Med. Chem., **Just Accepted Manuscript** • DOI: 10.1021/acs.jmedchem.9b00706 • Publication Date (Web): 28 Jun 2019

Downloaded from <http://pubs.acs.org> on June 29, 2019

Just Accepted

“Just Accepted” manuscripts have been peer-reviewed and accepted for publication. They are posted online prior to technical editing, formatting for publication and author proofing. The American Chemical Society provides “Just Accepted” as a service to the research community to expedite the dissemination of scientific material as soon as possible after acceptance. “Just Accepted” manuscripts appear in full in PDF format accompanied by an HTML abstract. “Just Accepted” manuscripts have been fully peer reviewed, but should not be considered the official version of record. They are citable by the Digital Object Identifier (DOI®). “Just Accepted” is an optional service offered to authors. Therefore, the “Just Accepted” Web site may not include all articles that will be published in the journal. After a manuscript is technically edited and formatted, it will be removed from the “Just Accepted” Web site and published as an ASAP article. Note that technical editing may introduce minor changes to the manuscript text and/or graphics which could affect content, and all legal disclaimers and ethical guidelines that apply to the journal pertain. ACS cannot be held responsible for errors or consequences arising from the use of information contained in these “Just Accepted” manuscripts.

1
2
3
4 Structure guided design, synthesis, and biological
5
6
7
8 evaluation of 2-(1H-Indol-3-yl)-1H-imidazol-4-
9
10
11
12 yl)(3,4,5-trimethoxyphenyl) Methanone (ABI-231)
13
14
15
16
17 analogs targeting the colchicine binding site in
18
19
20
21 tubulin
22
23

24 *Qinghui Wang^{†,φ,Π}, Kinsie E. Arnst^{†,Θ,Π}, Yuxi Wang^{‡,Π}, Gyanendra Kumar[§], Dejian Ma[†], Stephen*
25
26 *W. White[§], Duane D. Miller[†], Weimin Li^{‡,*}, Wei Li^{†,*}*

27
28
29 †Department of Pharmaceutical Sciences, College of Pharmacy, University of Tennessee Health
30
31 Science Center, Memphis, TN 38163, United States. ‡Department of Respiratory and Critical Care
32
33 Medicine, West China Hospital, Sichuan University, Chengdu, Sichuan 610041, §Department of
34
35 Structural Biology, St. Jude Children's Research Hospital, Memphis, TN 38105, United States.
36
37
38

39 *Corresponding author:

40
41
42 Wei Li, Ph.D., Department of Pharmaceutical Sciences, University of Tennessee Health Science
43
44 Center, Memphis, TN 38163. Email: wli@uthsc.edu, Tel: 901-448-7532, FAX: 901-448-6828.
45

46
47 Weimin Li, West China Hospital, Sichuan University, Chengdu, Sichuan 610041, China. Email:
48
49 weimin003@scu.edu.cn.
50
51
52
53
54
55
56
57
58
59
60

1
2
3 ABSTRACT: ABI-231 is a potent, orally bioavailable tubulin inhibitor that interacts with the
4 colchicine binding site and is currently undergoing clinical trials for prostate cancer. Guided by
5 the crystal structure of ABI-231 in complex with tubulin, we performed structure-activity
6 relationship (SAR) studies around the 3-indole moiety that led to the discovery of several potent
7 ABI-231 analogs, most notably **10ab** and **10bb**. The crystal structures of **10ab** and **10bb** in
8 complex with tubulin confirmed their improved molecular interactions to the colchicine site. *In*
9 *vitro*, biological studies showed that new ABI-231 analogs disrupt tubulin polymerization,
10 promote microtubule fragmentation, and inhibit cancer cell migration. *In vivo*, analog **10bb** not
11 only significantly inhibits primary tumor growth and decreases tumor metastasis in melanoma
12 xenograft models, but also shows a significant ability to overcome paclitaxel resistance in a taxane-
13 resistant PC-3/TxR model. In addition, pharmacological screening suggested that **10bb** has a low
14 risk of potential off-target function.
15
16
17
18
19
20
21
22
23
24
25
26
27
28
29
30
31
32
33
34
35
36
37
38
39
40
41
42
43
44
45
46
47
48
49
50
51
52
53
54
55
56
57
58
59
60

INTRODUCTION

Microtubules are cylindrical polymers that are of great importance for many cellular functions such as cell division and the formation of the mitotic spindle, cell shape maintenance, and cell motility. Microtubules also play a critical role in the proliferation of cancer cells¹⁻³, and microtubule dynamics is therefore one of the most productive therapeutic targets for cancer treatment³. Microtubule-targeting agents (MTAs) can interfere with functions of microtubules to disrupt the formation of the mitotic spindle, eventually leading to mitotic arrest at the metaphase/anaphase transition. A large number of MTAs have now been discovered and many have been approved by the FDA for the treatment of different cancer types, such as prostate cancer, breast cancer, lung cancer and ovarian cancer⁴. Based on their effects on microtubule dynamics, MTAs are generally classified into two categories: microtubule-stabilizing and microtubule-destabilizing agents. Microtubule-stabilizing agents such as epothilone, ixabepilone, paclitaxel, docetaxel, and cabazitaxel bind to polymerized tubulin proteins and enhance microtubule polymerization. On the contrary, microtubule-destabilizing agents such as colchicine and vinca alkaloids inhibit the polymerization of microtubules⁵.

The MTAs have achieved great success in cancer treatment for many types of cancers. However, drug-resistance is acquired over the course of treatment and becomes a significant clinical limitation. It is estimated that more than 1.7 million new cancer cases will be diagnosed in United States in 2019, and developing new anticancer agents to treat resistant phenotypes is therefore urgently needed⁶⁻⁷. Mechanisms that mediate drug-resistance against MTAs include, but are not limited to the overexpression of membrane-bound drug efflux proteins, such as P-glycoprotein (P-gp); the overexpression of certain β -tubulin isotypes; and tubulin protein mutations⁸⁻⁹. Taxanes and vinca alkaloids, are especially susceptible to efflux by ATP-binding cassette (ABC)

transporters and are less effective against cells overexpressing the tubulin β -III isotype¹⁰⁻¹².

The colchicine binding site is one of the well-documented binding sites in tubulin and located at the interface between α and β -tubulin heterodimers¹³. Colchicine binding site inhibitors (CBSIs, examples are listed in **Figure 1**) mechanistically decrease cellular motility, alter cell morphology, impair protein assembly, and arrest mitosis¹⁴⁻¹⁵. Colchicine (**Figure 1**) is a secondary metabolite isolated from natural sources and has wide-scope mechanisms of action. Unfortunately, it induces systemic toxicities and multi-organ dysfunction in a clinical trial for cancer treatment¹⁴, and thus is not currently approved by the FDA for cancer treatment. Other than colchicine and its derivatives, a number of other CBSIs have also been reported in the past decades, some examples are listed in **Figure 1**. Encouragingly, extensive preclinical studies have strongly suggested that CBSIs are effective in suppressing the overexpression of tubulin isotypes and surmount drug-resistance mediated by P-gp, MRP1, and MRP2¹⁶⁻¹⁸.

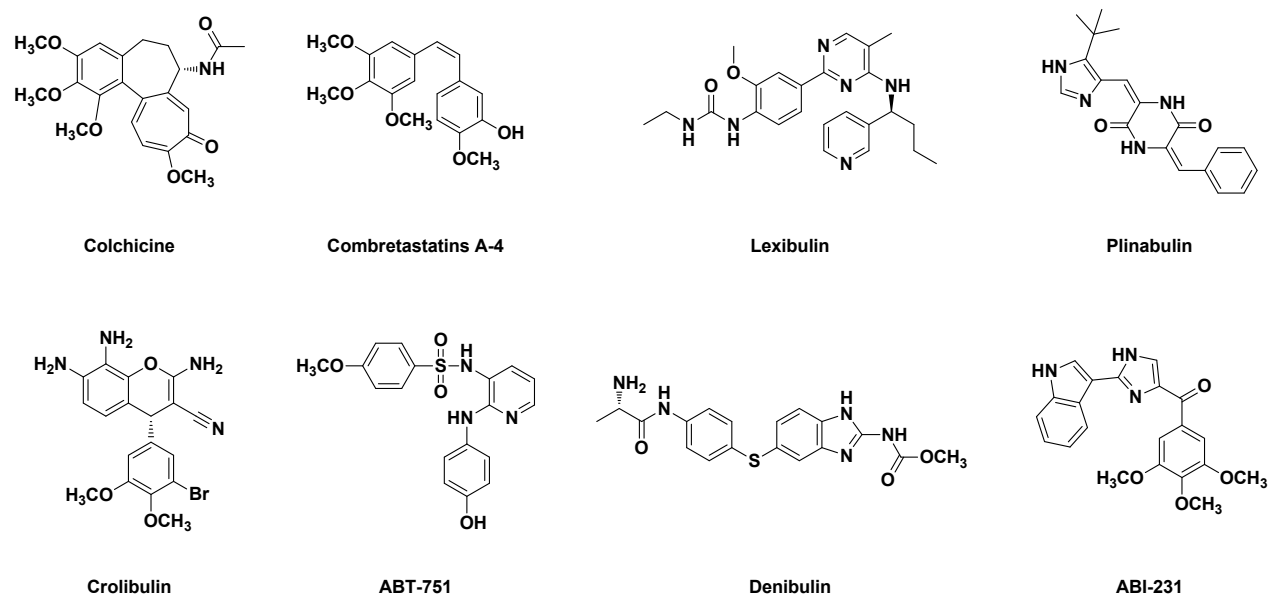


Figure 1. Examples of microtubule inhibitors that target colchicine binding sites in tubulin.

1
2
3 In our prior reports, we have described the discovery of several scaffolds of potent tubulin
4 inhibitors, including SMARTs, RABIs, ABIs, and IBIs¹⁹⁻²⁴. The SMART structure is our initially
5 discovered scaffold that exhibited nanomolar range antiproliferative activities against a panel of
6 cancer cell lines and showed promising *in vivo* activities in both melanoma and prostate xenograft
7 models^{19,25-27}. Subsequent structural modification of the SMART scaffold by replacing the central
8 thiazole ring with a more metabolically stable imidazole ring resulted in the discovery of 2-aryl-
9 4-benzoyl-imidazole (ABI-I/II) pharmacophores. ABI-I/IIs not only showed more potent activities
10 but also improved bioavailability in comparison with SMARTs¹⁹⁻²⁰. The ABI-III's pharmacophore
11 differed from ABI-I/IIs in having bicyclic heterocycles²¹⁻²², which are versatile moieties in
12 medicinal chemistry²⁸. ABI-III exhibited more potent antiproliferative activity (IC₅₀ values are in
13 low single-digit nanomolar range) than ABI-I/IIs. Rotation of the imidazole ring in ABI-I/IIs led
14 to the establishment of reverse ABIs (RABIs) which maintain comparable antiproliferative
15 potency²³. Substituting the central imidazole ring and the carbonyl linker in ABI-III with bicyclic
16 heterocycles provided the IBIs, which displayed similar potency to that of ABI-III²⁴. SMARTs,
17 ABIs, RABIs, and IBIs share the same mechanism of action: binding to the colchicine binding site
18 in tubulin and inhibiting tubulin polymerization. Interestingly, they are all effective against
19 multidrug-resistant cell lines and can circumvent P-gp mediated drug resistance²⁰⁻²². Amongst all
20 the scaffolds, ABI-231, a member of the ABI-III class, displays optimum activity and has an
21 average IC₅₀ value of 5.2 nM against a large panel of cancer cell lines²⁹. Additionally, it was
22 revealed that ABI-231 inhibits the expression of tubulin βIII and βIV over other isotypes via
23 restoring the expression of miR-200c in a panel of pancreatic cancer cell lines, which supports the
24 ability of ABI-231 to surmount drug resistance to existing tubulin inhibitors³⁰. Recently, we
25 described a focused SAR investigation of the trimethoxyphenyl (TMP) moiety in ABI-231 that
26
27
28
29
30
31
32
33
34
35
36
37
38
39
40
41
42
43
44
45
46
47
48
49
50
51
52
53
54
55
56
57
58
59
60

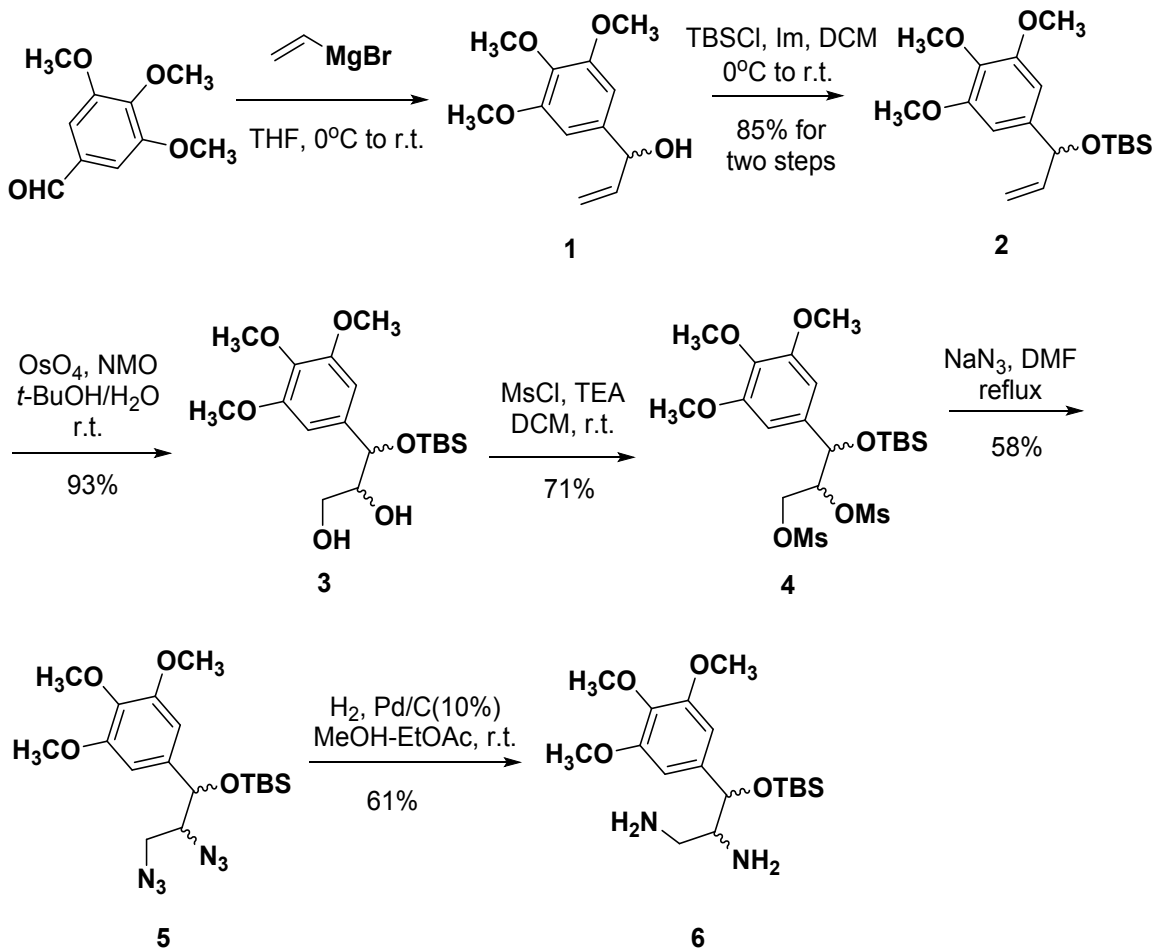
1
2
3 lead to a unique 3- methoxybenzo[4,5]-dioxene analog, which showed more potent
4 antiproliferative activity than ABI-231 ³¹. In this work, we describe an efficient synthesis of ABI-
5 231 that facilitated a SAR evaluation of the indole moiety, provide the molecular interactions and
6
7
8
9
10
11
12
13
14
15
16
17
18
19
20
21
22
23
24
25
26
27
28
29
30
31
32
33
34
35
36
37
38
39
40
41
42
43
44
45
46
47
48
49
50
51
52
53
54
55
56
57
58
59
60

lead to a unique 3- methoxybenzo[4,5]-dioxene analog, which showed more potent antiproliferative activity than ABI-231 ³¹. In this work, we describe an efficient synthesis of ABI-231 that facilitated a SAR evaluation of the indole moiety, provide the molecular interactions and rationales between tubulin proteins and ABI-231 or its two potent derivatives using X-ray crystallography, investigate the mechanism of action of the new analogs and determine their biological activities.

CHEMISTRY

To rapidly generate ABI-231 analogs modifying the indole moiety, we designed an efficient synthetic strategy illustrated in **Scheme S1**. Creation of the ABI-231 scaffold uses imidazoline cyclization, which requires a diamine intermediate and indolyl-3-carboxyaldehyde according to a reported methodology ³². In this method, it is crucial to accumulate a large quantity of the diamine intermediate, the synthesis of which was furnished in six steps and described in **Scheme 1**. Commercially available 3,4,5-trimethoxybenzaldehyde was treated with Grignard reagent vinylmagnesium bromide to generate the racemic mixture **1** ³³, which was subsequently treated with *tert*-butyldimethylsilyl chloride in the presence of imidazole to give **2**. **2** then underwent the Upjohn reaction in the presence of a catalytic equivalent of osmium tetroxide to obtain a mixture of diastereoisomers **3** in 79% yield over three steps. Diazide **5** was produced in two steps from **3** by following reported procedures ³⁴: mesylation of the diol **3** in the presence of methansulfonyl chloride and triethylamine yielded dimesylate **4** in 86% yield; **4** was then refluxed with sodium azide in DMF to give diazide **5** in 67% yield. Hydrogenation of diazide **5** in the presence of 10% Pd/C provided diamine **6** in 53% yield.

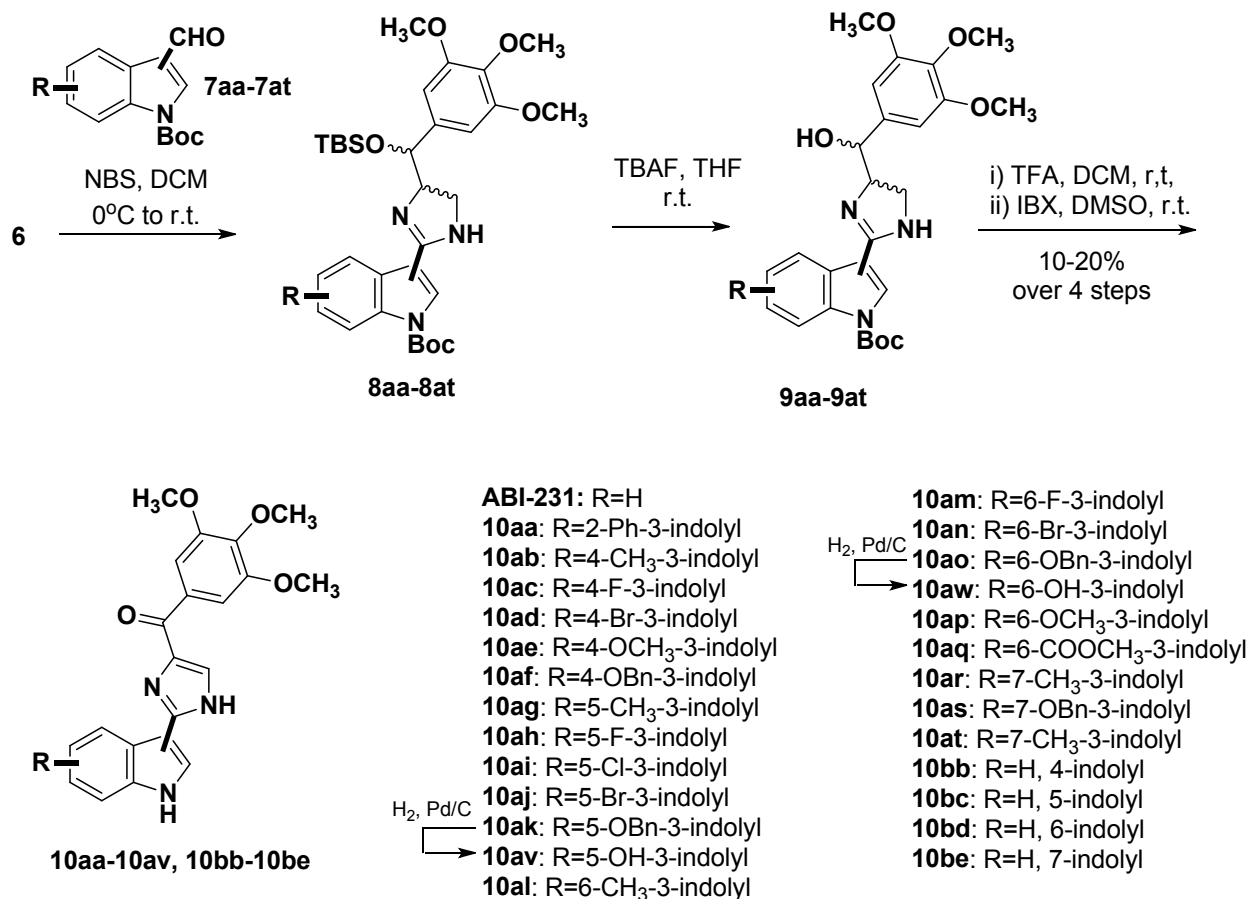
Scheme 1. Synthesis of diamine intermediate 6



With **6** in hand, syntheses of ABI-231 and its analogs was pursued as outlined in **Scheme 2** and furnished in 19% yield over four steps. Treatment of indole-3-carboxyaldehyde with di-*tert*-butyl dicarbonate gave **7**. In the presence of *N*-bromosuccinimide, **7** then reacted with diamine **6** at ice temperature to form imidazoline **8**, which was subjected to the deprotection of TBS in the presence of TBAF and the deprotection of Boc in the presence of TFA to provide **9** in two steps. ABI-231 was accomplished through simultaneous oxidation of the imidazoline to imidazole and the secondary alcohol to carbonyl in **9** in the presence of 3.0-5.0 equivalents of 2-iodoxybenzoic acid (IBX)³⁵. By following **Scheme 2**, we furnished twenty-six new ABI-231 analogs (**10aa-10av** and **10ba-10be**) in 10-20% yield over four steps. Hydrogenation of **10ak** and **10ao** afforded **10au** and

10av.

Scheme 2. Synthesis of ABI-231 analogs modifying the indole moiety



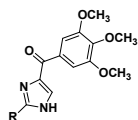
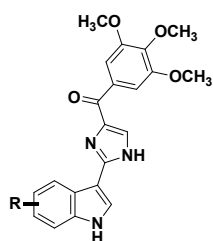
RESULTS AND DISCUSSION

SAR investigation. To compare to the antiproliferative potency of ABI-231 that was reported previously, the cytotoxicity of all new ABI-231 analogs were evaluated in human melanoma cell lines A375, WM164, and M14. Colchicine was used as a positive control and ABI-231 was used as a prototype for comparison. The antiproliferative activities of the compounds were evaluated in cell viability MTS assay. IC₅₀ values are reported in nM and were calculated from at least three independent experiments, each performed in quadruplicates using 96-well plates. Results from

these *in vitro* assays are shown in **Table 1**. ABI-231 has an IC₅₀ value ranging from 5.6-8.1 nM and is comparable to our previously reported data ²².

Table 1. *In vitro* growth inhibitory effects of ABI-231 analogs modifying the indole moiety (nM)

Compound	ID	R	A375	M14	WM164
	ABI-231	H	8.1 ± 1.6	5.6 ± 0.9	7.2 ± 0.9
	10aa	2-Ph	>1000	>1000	>1000
	10ab	4-CH ₃	1.8 ± 0.2	1.7 ± 0.2	3.2 ± 0.3
	10ac	4-F	7.2 ± 0.7	8.2 ± 0.9	ND
	10ad	4-Br	13.8 ± 1.7	10.4 ± 1.2	67.1 ± 14.5
	10ae	4-OCH ₃	>1000	>1000	>1000
	10af	4-OBn	>1000	>1000	>1000
	10ag	5-CH ₃	277.7 ± 36.3	177.4 ± 16.3	552.3 ± 108.3
	10ah	5-F	19.2 ± 1.5	18.0 ± 1.3	80.9 ± 16.6
	10ai	5-Cl	61.8 ± 9.3	64.9 ± 4.3	159.5 ± 24.1
	10aj	5-Br	164.2 ± 16.7	104.3 ± 5.9	441.7 ± 110.0
	10ak	5-OBn	>1000	>1000	>1000
	10au	5-OH	>1000	>1000	>1000
	10al	6-CH ₃	21.1 ± 3.9	21.7 ± 4.7	23.7 ± 6.1
	10am	6-F	17.5 ± 3.0	5.8 ± 0.8	10.3 ± 1.2
	10an	6-Br	67.8 ± 10.5	41.2 ± 7.5	55.4 ± 7.4
	10ao	6-OBn	>1000	>1000	>1000
	10av	6-OH	>1000	>1000	>1000
	10ap	6-OCH ₃	793.4 ± 89.9	879.8 ± 88.2	>1000
	10aq	6-COOCH ₃	>1000	>1000	>1000
	10ar	7-CH ₃	13.1 ± 1.3	10.8 ± 1.0	61.3 ± 11.0
	10as	7-OBn	>1000	>1000	>1000
	10at	7-OCH ₃	38.3 ± 3.7	34.1 ± 3.5	115.4 ± 25.0
	10bb	4-indolyl	3.6 ± 1.0	3.7 ± 0.8	1.6 ± 0.3
	10bc	5-indolyl	8.6 ± 3.3	18.5 ± 3.7	6.1 ± 1.2
	10bd	6-indolyl	8.0 ± 1.0	6.1 ± 1.1	3.8 ± 0.5
	10be	7-indolyl	285.5 ± 78.7	240.6 ± 38.1	435.8 ± 171.3
	Colchicine		14.1 ± 2.2	16.6 ± 1.5	10.8 ± 1.9



Twenty-two new analogs (**10aa** to **10at**) were synthesized to inspect substituent effects to the 3-indolyls. Compared to the prototype ABI-231, analog **10aa** with a bulky phenyl group on the 2-position of indole moiety showed essentially a total loss of activity with IC₅₀ values larger than 1

1
2
3 μM . This indicated that bulky substituents on the indole are not tolerated. Five analogs were
4 synthesized in the 4-position substituted series, including **10ab-10af** and **10au**. The best inhibitory
5 effect was observed in 4-methyl analog **10ab**, which has IC_{50} values ranging from 1.7-3.2 nM,
6 which is ~3-fold more potent than ABI-231. Analog **10ac** has a small substituent (4-F) and displays
7 nearly equipotent antiproliferative activity to that of ABI-231 with its IC_{50} values ranging from
8 7.2-8.2 nM. In contrast, **10ad**, an analog with a large-size halogen 4-bromo, has IC_{50} values
9 ranging from 10.4-67.1 nM and is 2-fold less potent than ABI-231. For analogs **10ae** with a 4-
10 methoxy group and **10af** with a 4-benzyloxy group, remarkable reductions of activities were
11 observed, their IC_{50} values are more than 1 μM . In general, 5-position substituted analogs show
12 substantially decreased antiproliferative activities in comparison with their corresponding 4-
13 position substituted counterparts. For example, the 5-fluoro analog **10ah** and the 5-bromo analog
14 **10aj** are 2-fold and 10-fold less potent than **10ac** and **10ad**, respectively. The 5-methyl analog
15 **10ag** has approximately 100-fold decreased antiproliferative activity compared to **10ab**. In this
16 series, the best activity was observed in the 5-fluoro analog **10ah**, which has IC_{50} values ranging
17 from 18.0-80.9 nM. It is surprising to find that hydrogenation of the bulky 5-benzyloxy analog
18 (**10ak**) to 5-hydroxy analog (**10au**) does not lead to any improvement of antiproliferative activity.
19 For the 6-position substituted analogs, similarly, bulky functional groups such as analogs **10ao**,
20 **10ap** and **10aq** lost activities (all have IC_{50} values of more than 1 μM) whereas small substituent
21 benefited the cytotoxicity, for example, 6-fluoro analog **10am**. The best activity in this series was
22 observed in **10am**, having IC_{50} values ranging from 5.8-17.5 nM. Hydrogenation of the bulky
23 benzyloxy to hydroxy on the 6-position did not provide any significant improvement of activity
24 (**10av**) neither. Among the 7-position substituted 3-indolyl analogs, **10ar** with a methyl
25 substitution possesses the most potent inhibitory effect (IC_{50} values range from 10.8-61.3 nM).
26
27
28
29
30
31
32
33
34
35
36
37
38
39
40
41
42
43
44
45
46
47
48
49
50
51
52
53
54
55
56
57
58
59
60

1
2
3 Interestingly, **10at** with a 7-methoxy substituent showed significantly stronger activity (IC_{50}
4 ranges from 34.1-115.4 nM) than its other position substituted counterparts (**10ae** and **10ap**).
5
6 Taken together, these SAR data revealed that small substituents (e.g. fluoro and methyl) are
7
8 strongly preferred over bulky functional groups on the 3-indolyl moiety, and modification at the
9
10 4-position generate the most potent analog (**10ab** in **Table 1**).
11
12
13
14

15
16 In addition, we previously reported a series of indolyl-imidazopyridines as CBSIs in 2015³⁶.
17
18 SAR studies in those compounds revealed that indolyl rotation significantly affects
19
20 antiproliferative activities. We hypothesized that this may also apply to ABI-231, considering its
21
22 overall structural similarity to the indolyl-imidazopyridines. To test this hypothesis, four ABI-231
23
24 analogs **10bb-10be** were synthesized (**Scheme 2**) and their *in vitro* growth inhibitory effects are
25
26 also shown in **Table 1**. In this series, 5- and 6-indolyl analogs **10bc** and **10bd** showed comparable
27
28 antiproliferative activities to that of ABI-231 and have IC_{50} values ranging from 6.1-18.5 and 3.8-
29
30 8.0 nM, respectively. The 7-indolyl analog **10be** was significantly less potent than ABI-231,
31
32 having IC_{50} values more than 100 nM. **10bb**, the 4-indolyl analog, showed approximately 2-fold
33
34 improvement of activity compared to ABI-231 and has IC_{50} values ranging from 1.6-3.7 nM.
35
36 Collectively, these data suggest that the antiproliferative activity of the ABI-231 scaffold is very
37
38 sensitive to the position in the indole moiety connecting to the central imidazole ring (e.g, 3-indole
39
40 and 4-indole are the best) and the position/size in this indole ring (e.g., a small, hydrophobic
41
42 substitution at the 3- or 4-position are strongly preferred).
43
44
45
46
47
48

49 **X-ray structures of ABI-231, 10ab and 10bb in complex with tubulin.** To understand the
50
51 molecular interactions between ABI-231 and tubulin protein, and the structural basis of the SAR
52
53 observed above, we first determined the crystal structure of the T2R-TTL (consisting of two α/β -
54
55 tubulin dimers, the stathmin-like protein RB3, and tubulin tyrosine ligase) in complex with ABI-
56
57
58
59
60

231 at a resolution of 2.6 Å (PDB code: 6O61). The crystallographic data and refinement statistics are shown in **Table 2**.

Table 2. X-Ray data collection and refinement statistics. ^a Values in parentheses are for highest-resolution shell.

	ABI-231 (PDB ID: 6O61)	Compound 10ab (PDB ID: 6O5N)	Compound 10bb (PDB ID: 6O5M)
Data collection			
Space group	P2 ₁ 2 ₁ 2 ₁	P2 ₁ 2 ₁ 2 ₁	P2 ₁ 2 ₁ 2 ₁
Cell dimensions			
<i>a</i> , <i>b</i> , <i>c</i> (Å)	105.26 157.09	105.30 157.76	104.97 157.72
	184.04	182.08	181.61
α , β , γ (°)	90 90 90	90 90 90	90 90 90
Resolution (Å)	50 - 2.60 (2.69 - 2.60) ^a	50 - 3.00 (3.11 - 3.00)	50 - 2.3 (2.37 - 2.3)
<i>R</i> _{meas}	0.116 (0.965)	0.150 (1.00)	0.113 (1.00)
<i>I</i> / σ (<i>I</i>)	16.25 (2.0)	12.25 (2.0)	22.6 (3.0)
Completeness (%)	99.2 (99.5)	99.9 (100)	99.9 (99.8)
Redundancy	6.8 (6.9)	6.7 (6.8)	13.0 (13.1)
Refinement			
Resolution (Å)	39.83 - 2.60 (2.69 - 2.60)	41.78 - 3.00 (3.11 - 3.00)	49.76 - 2.3 (2.37 - 2.3)
No. reflections	92647 (8453)	58910 (4504)	135160 (12695)
<i>R</i> _{work} / <i>R</i> _{free}	0.2049 / 0.2452	0.2024 / 0.2452	0.1899 / 0.2233
No. atoms	17165	17476	17881
Protein	16695	17228	16860
Ligand/ion	236	207	253
Water	234	41	768
<i>B</i> factors			
Protein	55.27	65.25	43.65
Ligand/ion	55.85	48.52	42.35
Water	40.72	47.30	41.74
R.m.s. deviations			
Bond lengths (Å)	0.005	0.004	0.004
Bond angles (°)	1.14	1.03	1.05
Ramachandra Plot			
Favoured (%)	97.99	96.10	98.18
Allowed (%)	1.92	3.71	1.77
Outliers (%)	0.09	0.19	0.05

1
2
3 The structure was clearly resolved (**Figure 2A**) and revealed that ABI-231 is bound at the
4 colchicine binding site at the interface of α and β -tubulin opposite the GTP that also binds at this
5 interface (**Figure 2B** and **2C**). It is positioned to make three hydrogen bonds with tubulin; the
6 carbonyl with the main chain NH of β -Asp249, the imidazole NH with the main chain C=O of α -
7 Thr179, and the indole NH with the main chain C=O of β -Asn347 and α -Thr178 through a water
8 “bridge”. The trimethoxyphenyl moiety of ABI-231 occupies a deep pocket lined by β -Tyr200, β -
9 Val236, β -Cys239 and β -Leu253. The imidazole ring is sandwiched between the side chains of β -
10 Leu246 on one side and β -Ly252 and β -Asn256 on the other side. The indole ring occupies a
11 pocket lined by β -Asn256, β -Met257, β -Ala314, β -Lys350, β -Lys350, and α -Val181. Note that
12 ABI-231 mostly interacts with the β -tubulin, but it also makes two interactions with the α -tubulin
13 (α -Thr179 and α -Thr178) across the interface. Thus, the compound acts like glue to increase the
14 α - and β -interaction. ABI-231 shares a similar binding pose to that of colchicine (**Figure S1A**),
15 indicating that the two compounds share a similar mode of inhibition.
16
17
18
19
20
21
22
23
24
25
26
27
28
29
30
31
32
33
34
35
36
37
38
39
40
41
42
43
44
45
46
47
48
49
50
51
52
53
54
55
56
57
58
59
60

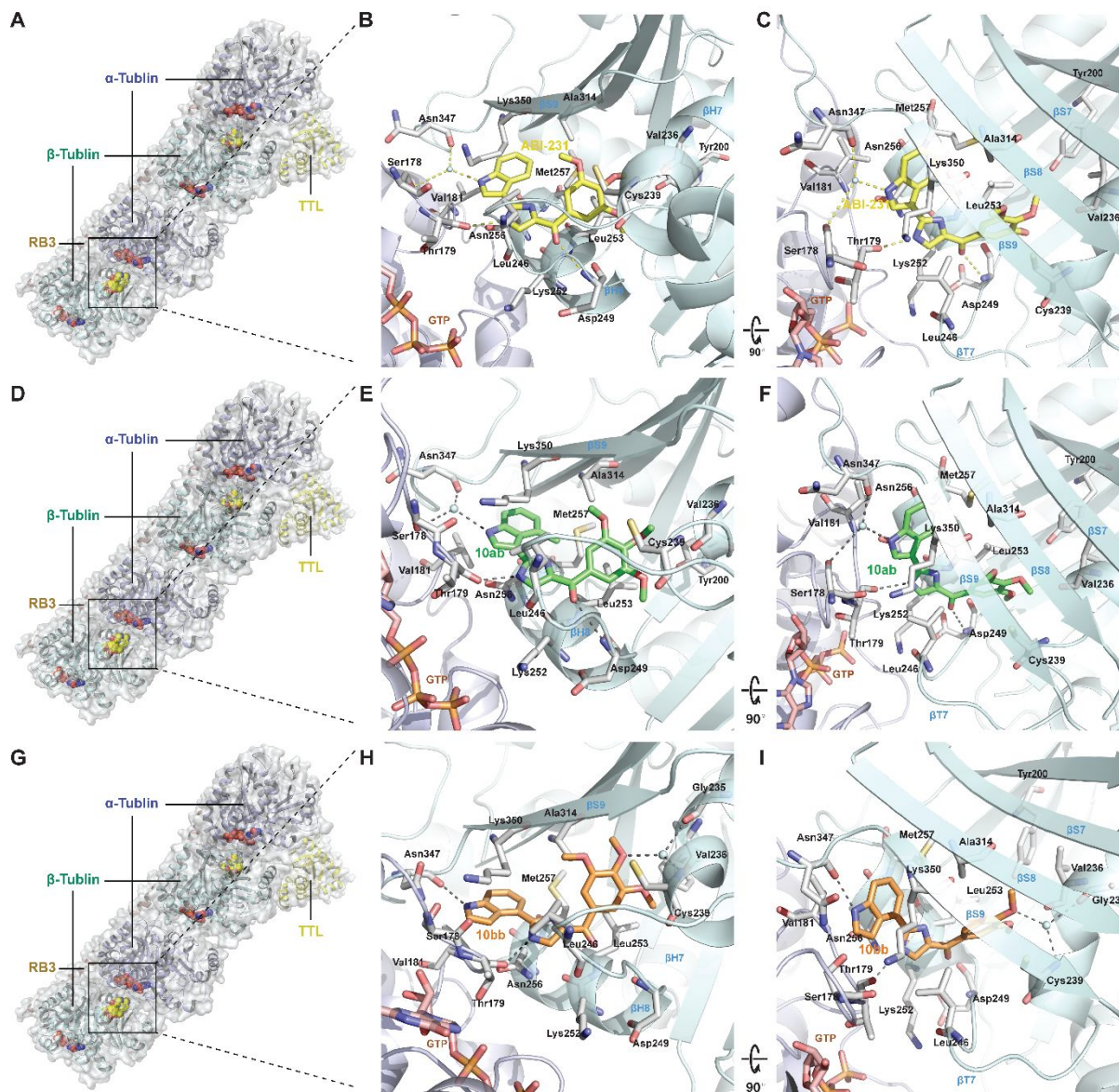


Figure 2. Complex structures of ABI-231 (6O61) and the new analogs **10ab** (6O5N) and **10bb** (6O5M) with tubulin protein. (A, D, G) overall crystal structure of the three compounds in complex with tubulin proteins. (B, E, H) detailed interactions between ABI-231, **10ab**, and **10bb** and tubulin (ABI-231 is in yellow stick representation, **10ab** is in green stick representation, and **10bb** is in orange stick representation). (C, F, I) 90-degree counterclockwise rotation view of the corresponding structures along x axis.

1
2
3 To investigate the prominent potencies of **10ab** and **10bb**, we also solved the crystal structures
4 of these compounds in complexes with tubulin protein (PDB code: 6O5N for **10ab**, 6O5M for
5 **10bb**). The crystallographic data and structure refinement statistics for **10ab** and **10bb** in complex
6 with tubulin are also shown in **Table 2**, and the electron density maps are shown in **Figure S2B**
7 and **S2C**, along with the electron density map for ABI-231 (**Figure S2A**). Similar to ABI-231,
8 **10ab** and **10bb** both bound to the colchicine binding site of tubulin and overlapped well with
9 colchicine (**Figure S1B** and **S1C**). **10ab** shows similar hydrogen bonding interactions to that of
10 ABI-231 and its increased activity can be attributed to the additional van der Waal interactions
11 afforded by the extra 4-methyl group that fills a small cavity in the ABI-231 complex bounded by
12 β -Leu253, β -Met257 and β -Ala314 (**Figure 2D to 2F**). **10bb** as a 4-indole compound shares the
13 main chain ABI-231 hydrogen bonding interactions with α -Thr179 and β -Asp249. Although the
14 hydrogen bonding to β -Asp249 is weakened compared with that in ABI-231 or **10ab**, the rotated
15 indole now allows a direct hydrogen bond between the indole NH and the main chain C=O of β -
16 Asn347 rather than the water mediated hydrogen bond seen in ABI-231 (Figure 2B and 2C). This
17 direct hydrogen bonding interaction also pull the **10bb** slightly up from the pocket where the TMP
18 moiety occupies, allowing a separate water-bridged hydrogen bonding network between the
19 middle methoxy oxygen to the backbone NH in β -Cys239 and CO in β -Gly235. This water
20 molecule has also been seen in a number of previously reported high resolution crystal structures
21 with another scaffold of CBSIs³⁷. Collectively, the direct hydrogen bond from the 4-indole moiety,
22 the added water-bridged hydrogen bond at the TMP pocket, and the ability of the rotated indole to
23 still occupy its binding pocket are likely to explain its increased activity. Both ABI-231 and its
24 new analogs binding are not compatible with the original straight conformation of tubulin protein.
25 Specifically, the curve-to-straight transition of tubulin is hindered by steric clashes between ABI-

1
2
3 231/**10ab/10bb** and the surrounding secondary elements (**Figure S3**), which is consistent with
4
5 previous reports^{13,38}.
6
7

8
9 **New ABI-231 analogs showed potent activities against NCI-60 panel cell lines.** Besides their
10 excellent antiproliferative activities observed in melanoma cell lines as tested in our lab, **10ab**,
11 **10bb**, and **10bd** were also tested against NCI-60 cell lines in both one-dose and full 5-dose assays.
12
13 The compounds effectively inhibited cancer cell growth in a variety of cancer types and were
14
15 particularly active against leukemia, colon, and prostate cancer (**Figure S4A**). They also produced
16
17 IC_{50} values in the low nanomolar range against the vast majority of the NCI-60 cell lines (**Figure**
18
19 **S4B**). It is clear that the new ABI-231 analogs **10ab**, **10bb**, and **10bd** all exhibit strong inhibitory
20
21 effects against a wide range of cancers.
22
23
24
25
26
27

28
29 **Inhibition of tubulin polymerization.** We next determined the effects of the most potent new
30 analogs (**10ab** and **10bb**) for their ability to inhibit tubulin polymerization, the primary
31 mechanisms of action of ABI-231. In a cell-free purified tubulin polymerization assay, 10 μ M
32 concentrations of **10ab** and **10bb** were evaluated against vehicle control and docetaxel, a well-
33 documented inducer of tubulin polymerization. **Figure 3A** clearly shows that compounds **10ab**
34 and **10bb** potently inhibited tubulin polymerization, while the vehicle experienced an initial and
35 rapid increase in polymerization and docetaxel strongly and consistently promoted polymerization.
36
37 The effects on microtubule networks were then observed by immunofluorescence via confocal
38
39 microscopy. Microtubule morphology in WM164 cells was visualized after 18 h of treatment of
40
41 with 100 nM of **10ab**, **10bb**, docetaxel, or untreated control cells. As shown in **Figure 3B**, **10ab**
42 and **10bb** dramatically disrupt microtubules, resulting in fragmentation and disassembly.
43
44 Docetaxel works in the opposite manner, causing hyperpolymerization and the formation of dense,
45
46 aggregated bundles of microtubules. These mechanistic studies confirm a mode of action by which
47
48
49
50
51
52
53
54
55
56
57
58
59
60

these compounds induce depolymerization of tubulin and disturb microtubule networks by interacting with the colchicine binding site.

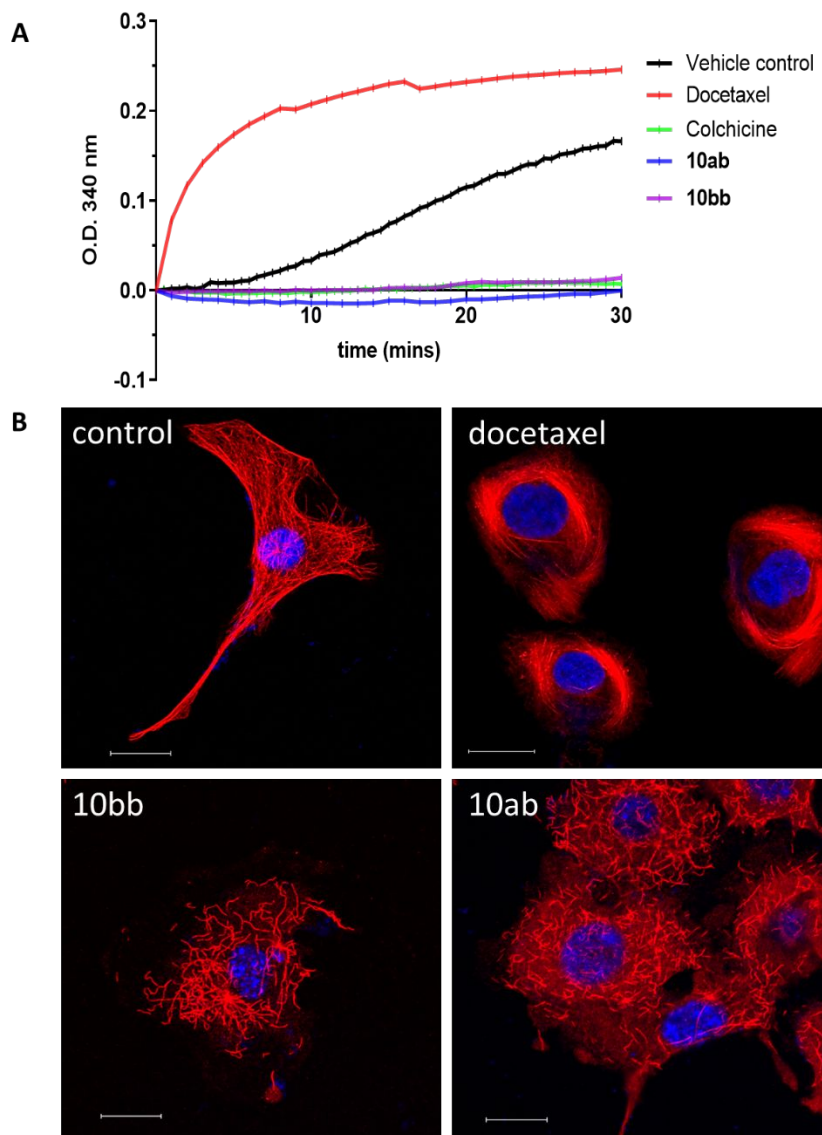


Figure 3. New ABI-231 analogs inhibit tubulin polymerization. (A) Polymerization of purified tubulin in a cell-free assay. Tubulin (3.33 mg/mL) was exposed to vehicle control or 10 μ M of the compounds ($n = 2$). Absorbance at 340 nm was monitored at 37 $^{\circ}$ C every minute for 30 min. (B) Effect on microtubules of WM164 cells following 18 h exposure to 100 nM of **10ab**, **10bb**, docetaxel or vehicle control. Confocal microscopy was utilized to visualize the microtubules

1
2
3 following immunofluorescent staining. Microtubules are shown in red and DNA is shown in blue.

4
5 Scale bar = 20 μm .
6
7

8
9 **In vitro inhibition of cancer growth and migration.** The long-term inhibitory growth effects
10 of **10ab** and **10bb** were tested in A375 cells in an anchorage-dependent colony formation assay.
11 The visual result and quantitative data are shown in **Figure 4A** and **4B**. While the vehicle control
12 treated cells averaged 199.3 ± 10.7 colonies after 12 days, both **10ab** and **10bb** significantly
13 inhibited colony number, with an average of 81.7 ± 7.8 and 128.3 ± 9.1 colonies, respectively. This
14 represents a 59.0% and 35.6% decrease, respectively, from the control. These compounds out-
15 performed colchicine, which averaged 150.0 ± 5.3 colonies, corresponding to a 24.7% decrease in
16 colony number. Tubulin and microtubule function are also implicated in cell migration and
17 motility. Therefore, we assessed the effect of **10ab** and **10bb** in a wound healing assay. After
18 removing a confluent monolayer of adherent A375 or RPMI7951 melanoma cells, the remaining
19 cells were treated for 18-22 h with 5 or 25 nM of **10ab**, **10bb**, or colchicine and compared against
20 untreated control cells. The total closure was calculated as a percentage of the total wound area
21 after treatment compared to the total area of removed cells immediately prior to treatment. In A375
22 and RPMI7951 cell lines, the control cells were able to efficiently migrate into the wound channel
23 apprehended, recovering $60.7\% \pm 3.5\%$ and $71.8\% \pm 1.8\%$ of the area, respectively (**Figure 4C**
24 and **4D**). Following 5 nM treatment, A375 cells only migrated into $48.5\% \pm 1.6\%$, $38.5 \pm 2.2\%$,
25 and $46.0\% \pm 1.4\%$ of the wound area for **10ab**, **10bb** and colchicine, respectively (**Figure 4C** and
26 **4D**). At higher concentrations of 25 nM, greater inhibition was observed, where **10ab** treated cells
27 recovered $25.9\% \pm 1.6\%$, **10bb** recovered $38.5\% \pm 2.2\%$, and colchicine treated cells recovered
28 $20.7\% \pm 2.2\%$ ($P < 0.0001$). A significant difference was also observed in RPMI7951 cells treated
29 at 25 nM of **10ab**, **10bb** or colchicine, leading to wound closure averaging $35.6\% \pm 6.6\%$, 35.0%
30
31
32
33
34
35
36
37
38
39
40
41
42
43
44
45
46
47
48
49
50
51
52
53
54
55
56
57
58
59
60

± 7.8%, and 42.8% ± 5.8%, respectively ($P = 0.0004$) (**Figure 4C** and **4D**). Normalized to the control cell lines, the average inhibition of cell migration for the treated cells was 53.5% for **10ab**, 52.8% for **10bb**, and 32.8% for colchicine. Taken together, these results demonstrate that **10ab** and **10bb** potently inhibit proliferation and migration of cancer cells *in vitro* at low nM concentrations.

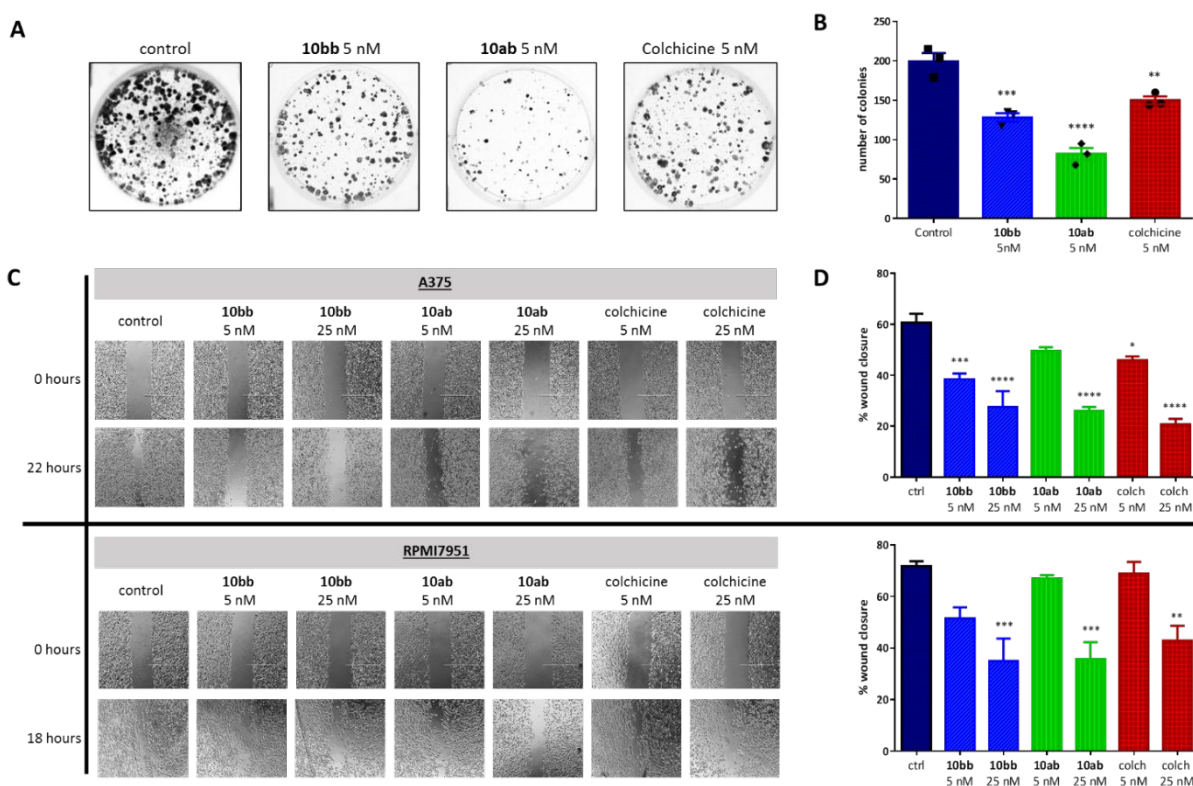


Figure 4. **10ab** and **10bb** inhibit colony growth and cancer cell migration. (A) Representative images of A375 colony formation for control or treated cells. (B) Quantification of colony numbers ($n = 3$). Statistical analysis was performed by ANOVA ($P < 0.0001$) followed by Dunnett's multiple comparison test. (C) Representative images of wound area in a scratch assay. Images were obtained after 18-22 h for A375 (top) or RPMI7951 (bottom) cells after treatment with 5 or 25 nM concentrations of **10ab**, **10bb**, colchicine, or untreated control. (D) Percentage of the wound closed

for A375 cells (top) or RPMI7951 cells (bottom) ($n = 3$). Area of the wound channel was calculated using ImageJ software. Statistical analysis was performed by ANOVA ($P < 0.0001$ for A375, $P = 0.0004$ for RPMI7951) followed by Dunnett's multiple comparison test.

***In vitro* microsomal stability.** To determine the most suitable candidates for *in vivo* efficacy studies, we examined the *in vitro* metabolic stabilities of the most potent analogs by measuring their half-life upon incubation with mouse, rat and human liver microsomes in the presence of an NADPH regeneration system. The results are summarized in **Table 3**. Overall, all three new ABI-231 analogs exhibited very good liver microsomal stabilities in three different species. **10bb**, which showed overall best *in vitro* potency and stability, was then selected for subsequent *in vivo* studies.

Table 3. Microsomal stability study of tested compounds in liver microsome of different species

Compounds	Metabolic Stability (Mouse)		Metabolic Stability (Rat)		Metabolic Stability (Human)	
	t1/2 (h)	Clint	t1/2 (h)	Clint	t1/2 (h)	Clint (ml/Min/Kg)
Verapamil	0.94±0.06	60.66	1.29±0.09	36.18	1.68±0.16	12.41
ABI-231	3.76±0.24	15.20	6.74±0.59	6.94	5.13±0.26	4.05
10ab	2.42±0.15	23.60	1.80±0.09	25.98	6.70±0.82	3.10
10bb	5.04±0.30	11.34	5.26±0.35	8.90	6.72±0.74	3.10
10bd	5.56±0.35	10.28	15.19±2.09	3.10	7.61±0.91	2.73

10bb inhibits melanoma tumor growth and metastasis in vivo. The anticancer efficacy of **10bb** was evaluated *in vivo* in two melanoma mouse models. All animal experiments performed in this report were conducted in compliance with the NIH and institutional guidelines, using approved animal protocols from the University of Tennessee Health Science Center. First, a xenograft model of nude mice challenged with A375 melanoma subcutaneously was treated every

1
2
3 other day via i.p. injection with 15 mg/kg or 30 mg/kg doses of **10bb**, paclitaxel, or a vehicle
4 solution only. After 20 days, the group receiving 15 mg/kg treatments of **10bb** achieved an average
5 tumor growth inhibition (TGI) of 82.3% and the group receiving the higher dose of 30 mg/kg
6 achieved a TGI of 90.6% (**Figure 5A**). Both treatment groups were more effective against the
7 xenograft tumors than the paclitaxel group, which had an average TGI of 68.6%. One-way
8 ANOVA analysis ($P = 0.0014$) followed by Dunnett's multiple comparison test also revealed that
9 there was a significant decrease compared to the control for both concentrations of **10bb** treated
10 groups ($P < 0.01$) and the paclitaxel treatment group ($P < 0.05$). Additionally, the final tumor
11 weights of the **10bb** 15 mg/kg and 30 mg/kg treated groups were 67.3% and 70.1% less than the
12 average final tumor weight for the control group, respectively (**Figure 5B**). One-way ANOVA (P
13 = 0.0024) followed by Dunnett's multiple comparison test confirmed statistical significance
14 between average tumor weights of the **10bb** treatment groups compared to the control ($P < 0.01$).
15 To investigate the ability of **10bb** to impede cancer metastasis, it was also tested in a lung
16 metastasis mouse model at 30 mg/kg doses in C57BL mice (**Figure 5C**). After inoculation with
17 melanoma cells via the lateral tail vein, mice were treated for two weeks at the same dosing
18 schedule as before. The average tumor index based on lung metastasis nodule size and the number
19 was 13.6 ± 2.9 for the control group and 2.6 ± 0.6 for the **10bb** treatment group. This was
20 significantly less than the control based on an unpaired student's t test ($P = 0.0013$) and represents
21 an 80.9% decrease in metastasis. Mouse weight and activity were monitored and for both the
22 xenograft model and lung metastasis model (**Figure 5D and 5E**). Pathohistological analysis was
23 performed on the major organs collected from both *in vivo* studies, including heart, liver, kidneys,
24 lungs, and spleen, to assess for acute toxicities. Sections stained with hematoxylin and eosin
25 revealed no apparent drug-related injury or morphological abnormalities in the cellular structure
26
27
28
29
30
31
32
33
34
35
36
37
38
39
40
41
42
43
44
45
46
47
48
49
50
51
52
53
54
55
56
57
58
59
60

of the various tissues in both the xenograft mouse model (**Figure 6A**) and the experimental lung metastasis mouse model (**Figure 6B**). Additionally, *in vitro* pharmacological profiling was utilized to identify undesirable off-target effects and assess the safety profile. **10bb** was evaluated at 1 μM (300~500 \times of its IC_{50} values against cancer cells as determined in **Table 1**) in the Safety47™ Panel which includes the assessment of the functional response of 47 major physiologically important targets across 78 assays (**Figure 6C**). Only a value higher than |70%| response is considered significant. **10bb** only showed hit responses in only 2 of the 78 assays, which were norepinephrine transporter (NET) and serotonin receptor 2B (HTR2B) antagonism. These findings support a good safety profile for **10bb** based on the *in vitro* and *in vivo* data.

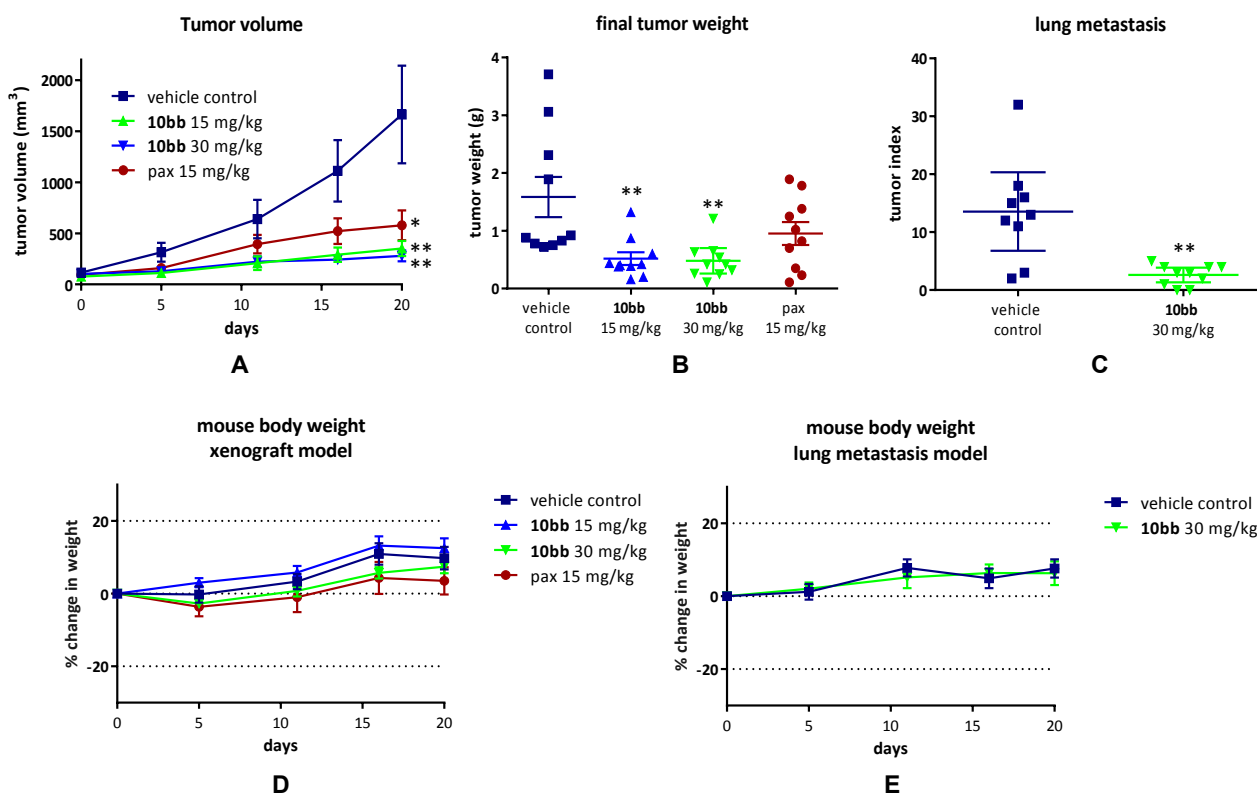


Figure 5. **10bb** inhibits melanoma tumor growth and metastasis *in vivo*. (A) Tumor volumes in an A375 xenograft model in nude mice (n = 10). Statistical significance for final tumor volume was determined by ANOVA ($P = 0.0014$) followed by Dunnett's multiple comparison test. (B)

Individual tumor weights. Error bars represent 95% CIs. Statistical significance was determined by ANOVA ($P = 0.0024$) analysis followed by Dunnett's multiple comparison test. (C) B16F10 lung metastasis in C57BL/6 mice. The graph represents the tumor index for mice ($n = 10$) and error bars represent 95% CIs. An unpaired student's t-test was performed to show statistical significance between the groups ($P = 0.0013$). Mouse body weights in the xenograft model (D) and lung metastasis model (E). Graph represents percent change in body weight compared to the starting weight.

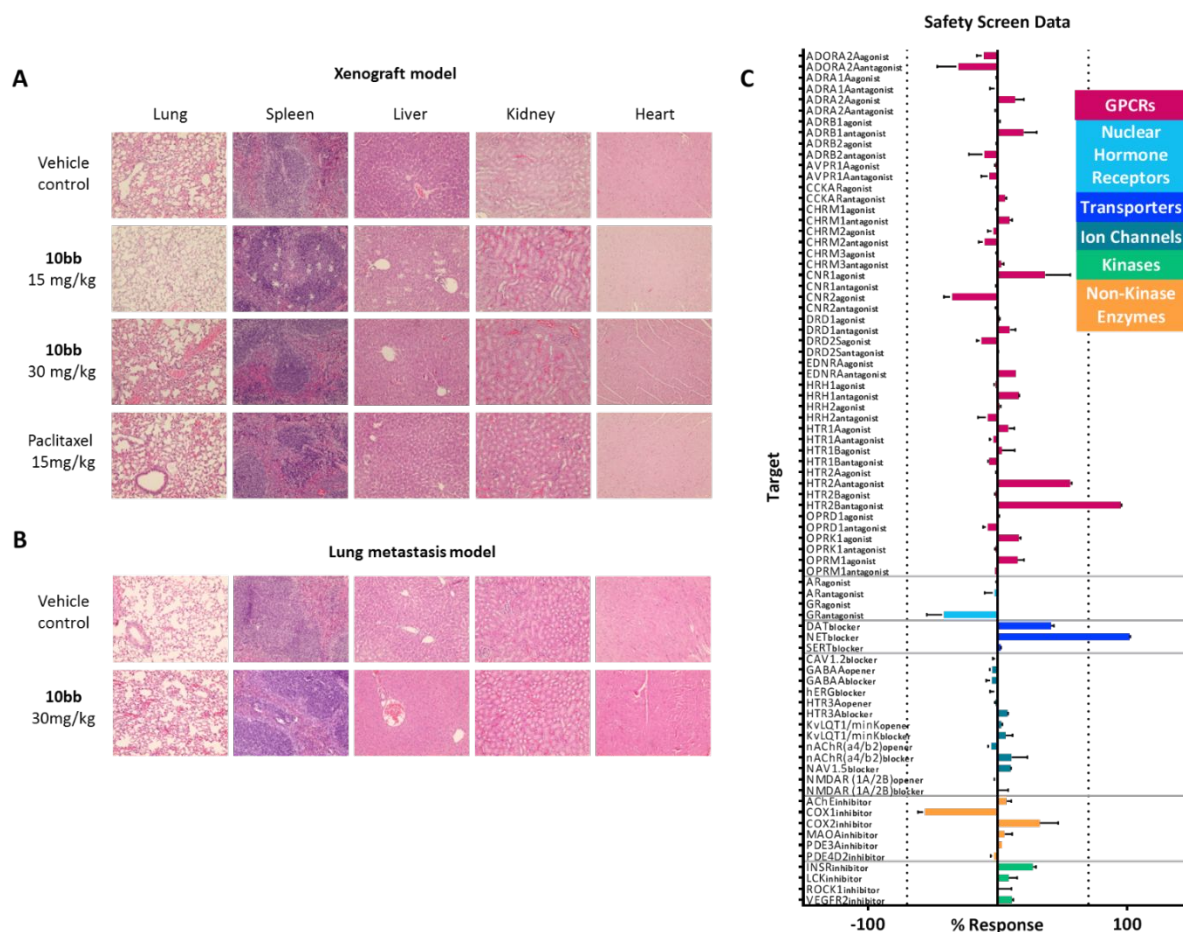


Figure 6. 10bb does not cause apparent toxicities to major organs. Pathological sections of major tissues (heart, kidney, liver, lung, and spleen) were obtained from the (A) A375 xenograft and (B) B16F10 lung metastasis studies. Organs were stained with Hematoxylin and Eosin (H&E) and

1
2
3 representative images were captured. (C) *In vitro* pharmacological profiling of **10bb** to assess
4 potential off-target effects to major targets at 1 μ M concentrations using the Safety47™ Panel (n
5 = 2). Graph represents mean percent response \pm range. Values in between -70% and +70%
6 (indicated with dashed lines) are considered insignificant.
7
8
9
10
11

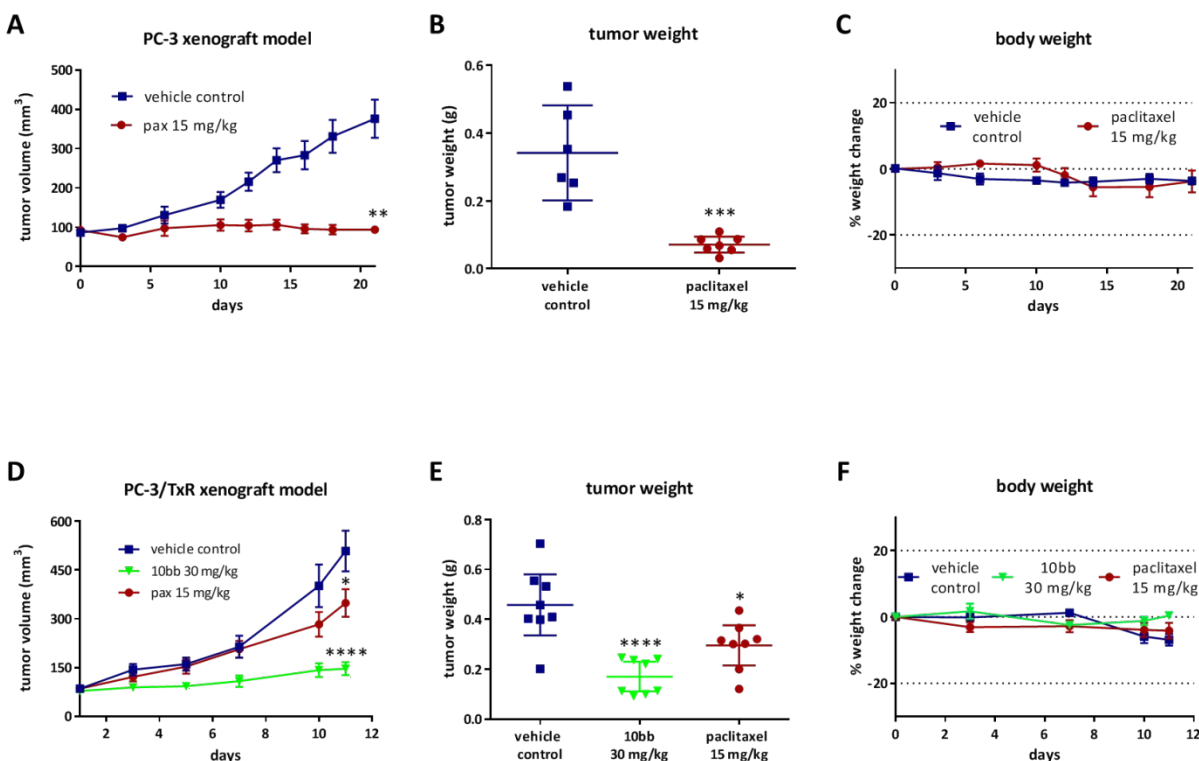
12
13 **10bb can circumvent paclitaxel resistance in vitro and vivo.** We next investigated the
14 potential for this scaffold of tubulin inhibitor in overcoming resistance mechanisms to which
15 taxanes are susceptible. We initially determined their activity against PC-3, DU-145, and their
16 corresponding paclitaxel resistant PC-3/TxR and DU-145/TxR cell lines *in vitro*. The resistance
17 index was determined by dividing the average IC₅₀ for the resistance cells by their parental cell
18 lines. We found that paclitaxel had a resistant index of 103.5 and > 869 for PC-3/TxR and DU-
19 145/TxR, respectively. Remarkably, **10bb** demonstrated greater potency against the resistant cells,
20 showing a resistance index of 0.7 and 2.2 (**Table 4**). Therefore, we wanted to confirm the ability
21 of **10bb** to escape paclitaxel resistance *in vivo*. First, we confirmed the efficacy of paclitaxel
22 against tumors that had not developed resistance. Nude mice bearing PC-3 xenograft tumors were
23 dosed with 15 mg/kg paclitaxel or the vehicle solution every other day for three weeks. As
24 expected, paclitaxel was effective in inhibiting tumor growth tumor growth, resulting in tumor
25 growth inhibition (TGI) of 101.2% ($P = 0.003$) (**Figure 7A**). Paclitaxel also caused an average
26 reduction in tumor weight by 79.3% which was significantly less than the vehicle treated group
27 ($P= 0.0003$) (**Figure 7B**). We next tested our compound **10bb** against a taxane-resistant PC-3 (PC-
28 3/TxR) model that was developed previously by others³⁹. At the same dosing concentrations and
29 frequency as the previous model, paclitaxel showed a marked decline in anticancer capabilities,
30 yielding a TGI of only 37.8% (**Figure 7D**) and a modest reduction in tumor weight of 34.5%
31 (**Figure 7E**). In contrast, 30 mg/kg treatments of **10bb** produced a significant reduction in tumor
32
33
34
35
36
37
38
39
40
41
42
43
44
45
46
47
48
49
50
51
52
53
54
55
56
57
58
59
60

growth by 83.8% and also decreased the average tumor weight by 62.8%. ANOVA analysis ($P < 0.0001$) followed by Dunnet's multiple comparison test confirmed a significant decrease in final tumor volume and weight ($P < 0.0001$) for the **10bb** treated groups. Animal activity and body weights were monitored and recorded throughout the experiment, and major deviations in body weight were not observed (**Figure 7C and 7F**).

Table 4. *In vitro* cytotoxicity of **10ab** and **10bb** in taxol resistant cancer cell lines.

Cell lines	IC ₅₀ ±SEM(nM)				
	10ab	10bb	Colchicine	Paclitaxel	Docetaxel
PC-3	5.2 ± 0.4	89.9 ± 6.3	10.4 ± 0.5	1.1 ± 0.2	0.5 ± 0.1
PC-3/TxR	3.9 ± 0.3	66.9 ± 4.4	37.4 ± 2.2	113.9 ± 4.3	27.9 ± 1.1
^a RI	0.8	0.7	3.6	103.5	55.8
DU-145	13.8 ± 1.0	169.1 ± 4.4	35.5 ± 3.5	1.15 ± 0.2	0.10 ± 0.01
DU-145/TxR	25.2 ± 2.0	379.1 ± 80.0	>1,000	>1,000	352.3 ± 118.2
^a RI	1.8	2.2	>28	>869	>3,523

^a RI: resistance index is calculated by dividing the IC₅₀ value of compound in resistant cell lines by the IC₅₀ in the corresponding parental cell lines.



1
2
3 **Figure 7. 10bb** is effective *in vivo* at inhibiting Taxol resistant tumor growth. Two models were
4 investigated in nude mice, one with parental PC-3 xenograft tumors and another with Taxol
5 resistant PC-3/TxR tumors. (A) Tumor volumes for the PC-3 xenograft model (n = 7). Statistical
6 analysis was performed by an unpaired t test, showing a significant difference for the final volumes
7 of the paclitaxel treated group compared to the control group ($P = 0.003$). (B) Final tumor weights
8 for the PC-3 xenograft model. Error bars represent 95% CIs. An unpaired t test showed a
9 significant difference between the paclitaxel and vehicle treated groups ($P = 0.0003$). (C) Mouse
10 body weights expressed as percent change compared to the starting weight in the PC-3 model. (D)
11 Tumor volumes for the PC-3/TxR xenograft model (n = 8). Statistical analysis was performed by
12 ANOVA ($P < 0.0001$) followed by Dunnett's multiple comparisons test for the final tumor
13 volumes. (E) Final tumor weights for PC-3/TxR mice. Error bars represent 95% CIs. Statistical
14 analysis was performed by ANOVA ($P = 0.0001$) followed by Dunnet's multiple comparisons test
15 (F) Body weights for PC-3/TxR mouse model. Graph represents mean body weight change as a
16 percentage compared to initial weight.

36 CONCLUSION

37
38
39 In this report, a SAR investigation of ABI-231 focusing on the modification of the indole moiety
40 is reported, revealing that **10ab** and **10bb** are more potent derivatives than the ABI-231 prototype.
41
42 The X-ray crystal structures of ABI-231, **10ab**, and **10bb** in complex with tubulin were obtained,
43
44 which confirmed that they directly bind to the colchicine site in tubulin, and revealed their
45
46 molecular mechanisms responsible for their improved interactions to tubulin proteins and the
47
48 resulted increased antiproliferative activities. We also demonstrated the abilities of the new
49
50 analogs to block tubulin polymerization and to inhibit cancer cell motility and migration. *In vivo*,
51
52 **10bb** effectively inhibited tumor growth and lung metastasis in melanoma xenograft and lung
53
54
55
56
57
58
59
60

1
2
3 metastasis models without showing signs of acute toxicity. More interestingly, **10bb** was highly
4
5 potent in inhibiting tumor growth of PC-3/TxR prostate xenograft tumors. This suggests, along
6
7 with the *in vitro* cell viability results, that **10bb** may circumvent certain types of MDR that taxanes
8
9 cannot escape. Taken together, these new ABI-231 analogs represent promising candidates for
10
11 further development as a new generation of tubulin inhibitors for cancer treatment.
12
13

14 15 16 **EXPERIMENTAL SECTION**

17
18
19 **General chemistry.** Tetrahydrofuran was distilled from sodium-benzophenone. All other
20
21 solvents and chemical reagents were obtained from commercial sources and directly used without
22
23 further purification. Glassware was oven-dried before use. All reactions were performed under an
24
25 argon atmosphere. TLC was performed on silica gel 60 GF254 and monitored under UV light or
26
27 visualized using phosphomolybdic acid reagent. Flash chromatography was performed on 230-
28
29 400 mesh silica gel (Fisher Scientific). Melting points were recorded on a MPA100 Automated
30
31 Melting Point Apparatus. NMR spectra were obtained on a Bruker Ascend 400 (Billerica, MA)
32
33 spectrometer or a Varian Inova-500 spectrometer (Agilent Technologies, Santa Clara, CA). HR-
34
35 MS were obtained on Waters Acquity UPLC linked to a Waters Acquity Photodiode Array
36
37 Detector and Waters qTof mass detector. All compounds reported herein with biological data had
38
39 purities $\geq 95\%$ as determined by HPLC. The purity of associated compounds was verified by the
40
41 HPLC study performed on BEH C18 (2.1 \times 50 mm, 1.7 μm) column using a mixture of solvent
42
43 acetonitrile/water (with 0.1% formic acid) at a flow rate of 0.3 ml/min and monitoring by UV
44
45 absorption at the appropriate wavelength. Chemical shifts are given in ppm. Tetramethylsilane
46
47 (TMS) is used as an internal reference for NMR spectra taken in chloroform-*d*. All coupling
48
49 constants (*J*) are given in Hertz (Hz).
50
51
52
53
54
55
56
57
58
59
60

1
2
3 **Synthesis of *tert*-butyldimethyl((1-(3,4,5-trimethoxyphenyl)allyl)oxysilane (2).** To a solution
4 of 3,4,5-trimethoxybenzaldehyde (30 g, 0.153 mol) in anhydrous THF (100 mL) at 0 °C under
5 argon was added vinylmagnesium bromide solution (168 mL, 0.168 mol, 1.0 M in THF) dropwise,
6
7 the resulting mixture was stirred for 1 h. On completion, reaction was quenched with saturated
8 NH₄Cl. The mixture was then extracted with ethyl acetate, washed with brine and dried with
9
10 anhydrous Na₂SO₄. The combined extracts were evaporated under vacuum to give **1** as crude oil
11 which was used directly for next step without purification³³. Imidazole (15.6 g, 0.229 mol) and
12
13 *tert*-butyldimethylsilyl chloride (34.4 g, 0.229 mol) were sequentially added to a solution of the
14 above crude oil in dichloromethane (150 mL) in a round bottom flask with stirring under argon.
15
16 The resulting suspension was stirred for 2 h. Water was then added and the mixture was extracted
17
18 with dichloromethane, washed with brine and dried with anhydrous Na₂SO₄. The combined
19
20 extracts were evaporated to give crude oil mixture which was directly used for next step without
21
22 purification.
23
24
25
26
27
28
29
30
31
32
33

34 **Synthesis of 3-((*tert*-butyldimethylsilyl)oxy)-3-(3,4,5-trimethoxyphenyl)propane-1,2-diol**
35 **(3).** To a solution of the compound **2** (44.0 g, 0.13 mol) in acetone (150 mL) was added *N*-
36 methylmorpholine *N*-oxide (22.9 g, 0.195 mol) and osmium tetroxide (40 mg, 0.157 mmol) in *tert*-
37 butanol (5 mL) at room temperature with stirring. After 48 h, acetone was removed under vacuum,
38
39 water and ethyl acetate were then added and the organic phase was separated, washed with brine
40
41 and dried with Na₂SO₄. Evaporation under vacuum gave the oily residue that was purified with
42
43 flash chromatography on silica. Elution with hexane/ethyl acetate (2:1-1:1) gave diol **3** as colorless
44
45 oil (45.1 g, 79% for three steps). ¹H NMR (400 MHz, Chloroform-*d*) δ 6.55 (d, *J* = 3.9 Hz, 2H),
46
47 4.65 (dd, *J* = 35.9, 6.1 Hz, 1H), 3.84 (t, *J* = 1.9 Hz, 9H), 3.77 – 3.40 (m, 3H), 2.87 – 1.97 (m, 2H),
48
49 0.91 (d, *J* = 0.7 Hz, 9H), 0.08 (d, *J* = 9.9 Hz, 3H), -0.07 – -0.19 (m, 3H).
50
51
52
53
54
55
56
57
58
59
60

1
2
3 **Synthesis of 3-((tert-butyldimethylsilyl)oxy)-3-(3,4,5-trimethoxyphenyl)propane-1,2-diyl**
4 **dimethanesulfonate (4).** To a solution of compound **3** (45.0 g, 0.12 mol) and Methanesulfonyl
5
6 chloride (23.4 mL, 0.30 mol) in anhydrous dichloromethane (100 mL) in a round bottom flask at
7
8 0 °C under argon, trimethylamine (36.9 mL, 0.26 mol) was added dropwise with vigorous stirring.
9
10 The resulting mixture was stirred overnight, water was then added and the reaction mixture was
11
12 extracted with dichloromethane, washed with brine and dried with anhydrous Na₂SO₄. The
13
14 combined extracts were evaporated under vacuum to give the oily crude, which was directly used
15
16 for next step without purification.
17
18
19
20
21

22 **Synthesis of tert-butyl(2,3-diazido-1-(3,4,5-trimethoxyphenyl)propoxy)dimethylsilane (5).**
23
24 To a solution of mesylate **4** (45.0 g, 0.085 mol) in anhydrous *N,N*-dimethylformamide (100 mL)
25
26 in a round bottom flask under argon, sodium azide (30 g, 0.46 mol) was added in portions with
27
28 stirring. The resulting mixture was refluxed for overnight. The precipitate was filtered off and
29
30 washed with dichloromethane. The combined filtration was evaporated under vacuum to give the
31
32 oily crude which was directly used for next step without purification.
33
34
35
36

37 **Synthesis of 3-((tert-butyldimethylsilyl)oxy)-3-(3,4,5-trimethoxyphenyl)propane-1,2-**
38 **diamine (6).** A suspension of azide **5** (20.0 g, 0.047 mol) and 10% Pd/C (0.2 g) in ethyl acetate-
39
40 methanol (1:1, 50 mL) was charged with hydrogen and stirred overnight, the reaction mixture was
41
42 filtered off and washed with dichloromethane-methanol (1:1). The combined filtration was
43
44 evaporated under vacuum to give the oily crude, which was purified with flash chromatography
45
46 on silica. Pure diamine **7** was eluted out with dichloromethane/methanol (15:0-15:1) as slightly
47
48 yellowish oil (10.6 g, 61%). ¹H NMR (400 MHz, Chloroform-*d*) δ 6.51 (d, *J* = 13.4 Hz, 2H), 4.45
49
50 (dd, *J* = 34.5, 5.1 Hz, 1H), 3.83 (d, *J* = 1.2 Hz, 9H), 2.97 – 2.46 (m, 3H), 0.90 (d, *J* = 10.8 Hz, 9H),
51
52 -0.17 (d, *J* = 8.5 Hz, 3H).
53
54
55
56
57
58
59
60

1
2
3 **General procedure for Boc protection of indolecarboxyaldehydes 7aa-7at and 7ba-7be.** To
4 a solution of the indoles (1.34 mmol) and 4-dimethylaminopyridine (65 mg, 0.54 mol) in
5 anhydrous dichloromethane (5 mL) under argon was added *di-tert*-butyl dicarbonate (351 mg, 1.61
6 mmol) with stirring. After 1 h, water was then added and the reaction mixture was extracted with
7 dichloromethane, washed with brine and dried with Na₂SO₄. Evaporation under vacuum gave the
8 crude solid residue **7aa-7at** and **7ba-7be** as white to yellowish solids that were used directly for
9 next step without purification.
10
11
12
13
14
15
16
17
18
19

20 **General procedure for cyclization to form imidazoline 8aa-8at and 8ba-8be.** A solution of
21 compound **6** (370 mg, 1.0 mmol) and boc-protected indole (1.1 mmol) in anhydrous
22 dichloromethane (10 mL) was stirred for 1 h under argon, then *N*-bromosuccinimide (151 mg, 0.85
23 mmol) was added at ice temperature and reaction was warmed to room temperature. After 4 h, the
24 reaction was quenched with saturated sodium thiosulfate solution and extracted with
25 dichloromethane for three times, washed with brine and dried with Na₂SO₄. The combined extracts
26 were evaporated to give crude oil **8aa-8at** and **8ba-8be**, which were used directly for next step
27 without purification.
28
29
30
31
32
33
34
35
36
37
38
39

40 **General procedure for removal of TBS protecting group.** To a stirred solution of compound
41 **8aa-8at** (0.5 mmol) in THF (5.0 mL) was added *tetra-n*-butylammonium fluoride (1.0 M in THF,
42 1.0 mL, 1.0 mmol) under argon. On completion, the reaction was quenched with water, extracted
43 with ethyl acetate for three times, washed with brine and dried with Na₂SO₄. The combined
44 extracts were evaporated to give crude oil **9aa-9at** and **9ba-9be**, which were used directly for next
45 step without purification.
46
47
48
49
50
51
52
53
54
55
56
57
58
59
60

General procedure for synthesis of 10ab-10at and 10ba-10be. To a stirred solution of compound **9** (0.1 mmol) in anhydrous dichloromethane (1.0 mL) was added trifluoroacetic acid (1.0 mL) under argon at room temperature. After 1 h, solvent was removed under reduced pressure to give crude solid that was directly used for next step without purification. To a stirred solution of the above crude in anhydrous dimethyl sulfoxide (2.0 mL) under argon was added 2-iodoxybenzoic acid (84 mg, 0.3 mmol) at room temperature. The reaction mixture was stirred overnight, extracted with ethyl acetate for three times, washed with brine and dried with Na₂SO₄. The combined extracts were evaporated to give crude solid, which was purified with flash chromatography on silica. Elution with hexane/ethyl acetate (4:1-1:1) gave pure compound **10ba-10be**.

General procedure for synthesis of 10au and 10av. To a stirred solution of compound **10ak** or **10ao** (0.05 mmol) in EtOAc-MeOH (3 mL, 1:1) was added catalytic equivalent of 10% Pd/C (0.0025 mmol) under argon at room temperature. The reaction was then charged with hydrogen, stirred and monitored by TLC. Upon the disappearance of starting material, the reaction mixture was filtered through celite and was with EtOAc. The combined solvents were evaporated to give crude solid, which was purified with flash chromatography on silica. Elution with Hexanes/ethyl acetate (1:1-1:4) gave pure compound **10au** or **10av**.

(2-(2-phenyl-1H-indol-3-yl)-1H-imidazol-4-yl)(3,4,5-trimethoxyphenyl)methanone (10aa). obtained as a yellowish solid (25.4 mg, 56.3% from **9aa**). ¹H NMR (400 MHz, Methylene Chloride-*d*₂ : Methanol-*d*₄ = 10: 1) δ 8.15 – 8.06 (m, 1H), 7.79 (s, 1H), 7.59 – 7.53 (m, 2H), 7.47 – 7.41 (m, 4H), 7.22 (dddd, *J* = 20.6, 8.1, 7.1, 1.2 Hz, 3H), 3.89 (s, 6H), 3.87 (s, 3H). ¹³C NMR (101 MHz, Methylene Chloride-*d*₂ : Methanol-*d*₄ = 10: 1) δ 183.58, 153.73, 142.58, 138.59, 136.68, 133.65, 132.38, 129.72, 129.63, 129.13, 128.11, 123.63, 121.59, 121.06, 111.94, 111.89,

1
2
3 107.17, 61.19, 56.78. HRMS: calculated for C₂₇H₂₄N₃O₄ [M+H]⁺ 454.1767, found 454.1759.
4
5 Purity: 95.0% by HPLC (R_t = 2.36 min).
6
7

8
9 **(2-(4-methyl-1H-indol-3-yl)-1H-imidazol-4-yl)(3,4,5-trimethoxyphenyl)methanone (10ab).**

10 obtained as a yellowish solid (23.2 mg, 59.2% from **9ab**). ¹H NMR (400 MHz, Methylene
11 Chloride-*d*₂: Methanol-*d*₄ = 10: 1) δ 7.78 (s, 1H), 7.36 (s, 1H), 7.22 (d, *J* = 16.4 Hz, 3H), 7.08 (t,
12 *J* = 7.6 Hz, 1H), 6.93 – 6.84 (m, 1H), 3.88 (d, *J* = 2.0 Hz, 9H), 2.50 (s, 3H). ¹³C NMR (101 MHz,
13 Methylene Chloride-*d*₂: Methanol-*d*₄ = 10: 1) δ 184.41, 153.78, 148.55, 142.68, 137.13, 136.97,
14 135.76, 133.67, 133.22, 131.08, 127.41, 127.24, 125.09, 125.06, 123.30, 122.79, 110.14, 110.09,
15 107.17, 106.73, 106.69, 61.21, 56.82, 21.07. HRMS: calculated for C₂₂H₂₂N₃O₄ [M+H]⁺ 392.1610,
16 found 392.1613. Purity: 99.2% by HPLC (R_t = 1.83 min).
17
18
19
20
21
22
23
24
25
26
27

28 **2-(4-fluoro-1H-indol-3-yl)-1H-imidazol-4-yl)(3,4,5-trimethoxyphenyl)methanone (10ac).**

29 obtained as a yellowish solid (18.4 mg, 46.5% from **9ac**). ¹H NMR (400 MHz, Chloroform-*d*) δ
30 8.04 (s, 1H), 7.71 (s, 1H), 7.24 (d, *J* = 8.1 Hz, 1H), 7.19 (s, 2H), 7.14 (td, *J* = 8.0, 5.2 Hz, 1H),
31 6.91 (dd, *J* = 12.7, 7.8 Hz, 1H), 3.90 (d, *J* = 1.1 Hz, 9H). ¹³C NMR (101 MHz, Chloroform-*d*) δ
32 182.71, 154.61, 153.21, 146.69, 142.09, 139.45, 139.35, 132.94, 127.76, 123.83, 123.75, 112.42,
33 112.23, 108.90, 106.73, 106.51, 106.31, 104.39, 61.02, 56.32. HRMS: calculated for C₂₁H₁₉FN₃O₄
34 [M+H]⁺ 396.1360, found 396.1370. Purity: 97.4% by HPLC (R_t = 2.52 min).
35
36
37
38
39
40
41
42
43
44

45 **(2-(4-bromo-1H-indol-3-yl)-1H-imidazol-4-yl)(3,4,5-trimethoxyphenyl)methanone (10ad).**

46 obtained as a yellowish solid (28.9 mg, 63.4% from **9ad**). ¹H NMR (400 MHz, Methylene
47 Chloride-*d*₂: Methanol-*d*₄ = 10: 1) δ 7.77 (s, 1H), 7.68 (s, 1H), 7.42 (d, *J* = 8.1 Hz, 1H), 7.34 (d, *J*
48 = 7.6 Hz, 1H), 7.26 (s, 2H), 7.06 (t, *J* = 7.9 Hz, 1H), 3.91 (s, 6H), 3.87 (s, 3H). ¹³C NMR (101
49 MHz, Methylene Chloride-*d*₂: Methanol-*d*₄ = 10: 1) δ 184.36, 153.80, 146.48, 142.67, 138.16,
50
51
52
53
54
55
56
57
58
59
60

1
2
3 133.68, 129.87, 125.75, 124.76, 123.88, 113.25, 112.31, 112.25, 107.15, 106.35, 61.20, 56.84.

4
5 HRMS: calculated for $C_{21}H_{19}BrN_3O_4$ $[M+H]^+$ 456.0559, found 456.0556. Purity: 98.6% by HPLC
6
7
8 (R_t = 1.89 min).

9
10
11 **(2-(4-methoxy-1H-indol-3-yl)-1H-imidazol-4-yl)(3,4,5-trimethoxyphenyl)methanone**

12
13 **(10ae)**. obtained as a yellowish solid (17.6 mg, 43.1% from **9ae**). 1H NMR (400 MHz, Chloroform-
14
15 *d* : Methanol- d_4 = 10: 1) δ 9.91 (s, 1H), 8.75 (s, 1H), 7.90 (s, 1H), 7.41 (d, J = 8.4 Hz, 1H), 7.30
16
17 (s, 2H), 7.26 (s, 2H), 6.70 (d, J = 8.4 Hz, 1H), 4.26 (s, 3H), 4.01 (s, 3H), 4.00 (s, 6H). ^{13}C NMR
18
19 (101 MHz, Chloroform-*d*) δ 181.65, 153.51, 151.42, 145.59, 143.17, 138.93, 131.25, 130.44,
20
21 128.59, 127.66, 124.71, 113.49, 107.27, 106.23, 102.57, 99.65, 61.05, 56.41, 56.09. HRMS:
22
23 calculated for $C_{22}H_{22}N_3O_5$ $[M+H]^+$ 408.1559, found 408.1540. Purity: 96.9% by HPLC (R_t = 2.00
24
25 min).

26
27
28
29
30
31 **(2-(4-(benzyloxy)-1H-indol-3-yl)-1H-imidazol-4-yl)(3,4,5-trimethoxyphenyl)methanone**

32
33 **(10af)**. obtained as a yellowish solid (32.9 mg, 70.0% from **9af**). 1H NMR (400 MHz, Chloroform-
34
35 *d*) δ 9.79 (s, 1H), 8.14 (d, J = 2.6 Hz, 1H), 7.60 (s, 1H), 7.55 – 7.50 (m, 2H), 7.38 (t, J = 7.4 Hz,
36
37 2H), 7.33 (d, J = 7.1 Hz, 1H), 7.29 (s, 2H), 7.18 – 7.07 (m, 2H), 6.75 (d, J = 7.2 Hz, 1H), 5.52 (s,
38
39 2H), 3.96 (s, 3H), 3.94 (s, 6H). ^{13}C NMR (101 MHz, Methylene Chloride- d_2) δ 183.51, 153.73,
40
41 151.84, 142.38, 139.56, 136.73, 134.10, 129.41, 129.04, 128.66, 126.85, 124.00, 114.88, 107.16,
42
43 107.09, 103.65, 71.70, 61.15, 56.78. HRMS: calculated for $C_{28}H_{26}N_3O_5$ $[M+H]^+$ 484.1872, found
44
45 484.1871. Purity: 98.7% by HPLC (R_t = 2.42 min).

46
47
48
49
50 **(2-(5-methyl-1H-indol-3-yl)-1H-imidazol-4-yl)(3,4,5-trimethoxyphenyl)methanone (10ag).**

51
52 obtained as a yellowish solid (23.8 mg, 60.7% from **9ag**). 1H NMR (400 MHz, Methylene
53
54 Chloride- d_2 : Methanol- d_4 = 10: 1) δ 8.03 (s, 1H), 7.88 (d, J = 1.6 Hz, 1H), 7.79 (s, 1H), 7.36 (dd,
55
56
57
58
59
60

J = 8.4, 1.5 Hz, 1H), 7.27 (s, 2H), 7.09 (d, J = 8.4 Hz, 1H), 3.92 (d, J = 1.6 Hz, 6H), 3.88 (d, J = 1.6 Hz, 3H), 2.62 – 2.40 (m, 3H). ¹³C NMR (101 MHz, Methylene Chloride-*d*₂ : Methanol-*d*₄ = 10: 1) δ 184.33, 153.77, 149.36, 142.51, 135.52, 134.01, 131.13, 126.56, 125.50, 125.01, 120.34, 112.08, 107.14, 106.03, 61.22, 56.79, 21.80. HRMS: calculated for C₂₂H₂₂N₃O₄ [M+H]⁺ 392.1610, found 392.1608. Purity: 100.0% by HPLC (R_t = 1.96 min).

(2-(5-fluoro-1H-indol-3-yl)-1H-imidazol-4-yl)(3,4,5-trimethoxyphenyl)methanone (10ah).

obtained as a yellowish solid (17.7 mg, 44.7% from **9ah**). ¹H NMR (400 MHz, Methylene Chloride-*d*₂ : Methanol-*d*₄ = 10: 1) δ 8.00 – 7.91 (m, 2H), 7.80 (s, 1H), 7.41 (dd, J = 8.9, 4.5 Hz, 1H), 7.30 (s, 2H), 7.01 (td, J = 9.0, 2.5 Hz, 1H), 3.92 (s, 6H), 3.88 (s, 3H). ¹³C NMR (101 MHz, Methylene Chloride-*d*₂ : Methanol-*d*₄ = 10: 1) δ 184.61, 160.45, 158.11, 153.75, 142.54, 134.00, 133.81, 127.77, 125.96, 125.85, 113.26, 113.17, 111.74, 111.48, 107.28, 106.92, 106.88, 106.21, 105.96, 61.22, 56.79. HRMS: calculated for C₂₁H₁₉FN₃O₄ [M+H]⁺ 396.1360, found 396.1371. Purity: 99.0% by HPLC (R_t = 1.94 min).

(2-(5-chloro-1H-indol-3-yl)-1H-imidazol-4-yl)(3,4,5-trimethoxyphenyl)methanone (10ai).

obtained as a yellowish solid (28.5 mg, 69.2% from **9ai**). ¹H NMR (400 MHz, Acetone-*d*₆) δ 10.93 (s, 1H), 8.64 (d, J = 2.2 Hz, 1H), 8.29 (s, 1H), 7.92 (s, 1H), 7.54 (d, J = 8.7 Hz, 2H), 7.23 (dd, J = 8.7, 2.1 Hz, 1H), 3.97 (s, 6H), 3.85 (s, 3H). ¹³C NMR (101 MHz, Acetone-*d*₆) δ 154.15, 142.94, 136.18, 134.44, 127.60, 126.71, 123.53, 121.78, 114.04, 114.00, 107.57, 60.71, 56.67. HRMS: calculated for C₂₁H₁₉ClN₃O₄ [M+H]⁺ 412.1064, found 412.1057. Purity: 99.1% by HPLC (R_t = 2.12 min).

(2-(5-bromo-1H-indol-3-yl)-1H-imidazol-4-yl)(3,4,5-trimethoxyphenyl)methanone (10aj).

obtained as a yellowish solid (26.9 mg, 58.9% from **9aj**). ¹H NMR (400 MHz, Methylene

1
2
3 Chloride- d_2 : Methanol- $d_4 = 10$: 1) δ 8.44 (dd, $J = 1.9, 0.8$ Hz, 1H), 7.90 (s, 1H), 7.80 (s, 1H), 7.39
4
5 – 7.26 (m, 4H), 3.93 (s, 6H), 3.88 (s, 3H). ^{13}C NMR (101 MHz, Methylene Chloride- d_2 : Methanol-
6
7 $d_4 = 10$: 1) δ 184.63, 153.78, 148.24, 142.61, 135.92, 133.91, 127.33, 127.10, 126.19, 123.58,
8
9 114.77, 113.96, 107.29, 106.30, 61.23, 56.84. HRMS: calculated for $\text{C}_{21}\text{H}_{19}\text{BrN}_3\text{O}_4$ $[\text{M}+\text{H}]^+$
10
11 456.0559, found 456.0570. Purity: 100.0% by HPLC ($R_t = 2.18$ min).
12
13
14

15
16 **(2-(5-(benzyloxy)-1H-indol-3-yl)-1H-imidazol-4-yl)(3,4,5-trimethoxyphenyl)methanone**

17
18 **(10ak)**. obtained as a yellowish solid (29.1 mg, 60.1% from **9ak**). ^1H NMR (400 MHz, Acetone-
19
20 d_6) δ 10.69 (s, 1H), 8.24 (dd, $J = 9.5, 2.5$ Hz, 2H), 7.93 (s, 1H), 7.59 – 7.46 (m, 4H), 7.46 – 7.35
21
22 (m, 3H), 7.35 – 7.28 (m, 1H), 6.98 (dd, $J = 8.8, 2.5$ Hz, 1H), 5.16 (s, 2H), 3.95 (s, 6H), 3.82 (s,
23
24 3H). ^{13}C NMR (101 MHz, Acetone- d_6) δ 183.75, 155.14, 154.15, 142.92, 138.97, 134.58, 133.03,
25
26 132.88, 129.20, 128.58, 128.47, 127.12, 126.57, 126.40, 114.10, 113.23, 113.18, 107.92, 107.32,
27
28 105.98, 71.25, 60.71, 60.54, 56.69. HRMS: calculated for $\text{C}_{28}\text{H}_{26}\text{N}_3\text{O}_5$ $[\text{M}+\text{H}]^+$ 484.1872, found
29
30 484.1896. Purity: 99.4% by HPLC ($R_t = 2.34$ min).
31
32
33
34

35
36 **(2-(6-methyl-1H-indol-3-yl)-1H-imidazol-4-yl)(3,4,5-trimethoxyphenyl)methanone (10al)**.

37
38 obtained as a yellowish solid (17.3 mg, 44.1% from **9al**). ^1H NMR (400 MHz, Methylene Chloride-
39
40 d_2) δ 8.06 (d, $J = 8.2$ Hz, 1H), 7.88 (s, 1H), 7.83 (s, 1H), 7.25 (s, 2H), 7.21 (s, 1H), 7.05 (d, $J = 8.0$
41
42 Hz, 1H), 3.87 (d, $J = 3.0$ Hz, 9H), 2.41 (s, 3H). ^{13}C NMR (101 MHz, Methylene Chloride- d_2) δ
43
44 183.51, 153.86, 148.33, 142.82, 137.43, 133.85, 133.46, 132.01, 125.84, 123.74, 123.03, 120.50,
45
46 112.28, 107.08, 106.16, 61.20, 56.83, 21.90. HRMS: calculated for $\text{C}_{22}\text{H}_{22}\text{N}_3\text{O}_4$ $[\text{M}+\text{H}]^+$ 392.1610,
47
48 found 392.1612. Purity: 98.4% by HPLC ($R_t = 1.92$ min).
49
50
51

52
53 **(2-(6-fluoro-1H-indol-3-yl)-1H-imidazol-4-yl)(3,4,5-trimethoxyphenyl)methanone (10am)**.

54
55 obtained as a yellowish solid (19.5 mg, 49.2% from **9am**). ^1H NMR (400 MHz, Methylene
56
57
58
59
60

1
2
3 Chloride- d_2 : Methanol- $d_4 = 10$: 1) δ 8.27 – 8.17 (m, 1H), 7.88 (d, $J = 2.1$ Hz, 1H), 7.79 (d, $J = 2.5$
4 Hz, 1H), 7.30 (d, $J = 2.1$ Hz, 2H), 7.15 (dt, $J = 9.6, 2.4$ Hz, 1H), 6.98 (ddd, $J = 9.6, 8.8, 2.4$ Hz,
5 1H), 3.91 (d, $J = 2.2$ Hz, 6H), 3.87 (s, 3H). ^{13}C NMR (101 MHz, Methylene Chloride- d_2 :
6 Methanol- $d_4 = 10$: 1) δ 184.67, 161.98, 159.62, 153.76, 148.67, 142.55, 137.37, 137.25, 134.00,
7 126.67, 126.64, 122.14, 122.10, 122.00, 110.09, 109.85, 107.27, 106.71, 98.65, 98.40, 61.23,
8 56.77. HRMS: calculated for $\text{C}_{21}\text{H}_{19}\text{FN}_3\text{O}_4$ $[\text{M}+\text{H}]^+$ 396.1360, found 396.1360. Purity: 98.4% by
9 HPLC ($R_t = 1.96$ min).

10
11
12
13
14
15
16
17
18
19
20 **(2-(6-bromo-1H-indol-3-yl)-1H-imidazol-4-yl)(3,4,5-trimethoxyphenyl)methanone (10an).**
21
22 obtained as a yellowish solid (26.3 mg, 57.6% from **9an**). ^1H NMR (400 MHz, Methylene
23 Chloride- d_2 : Methanol- $d_4 = 10$: 1) δ 8.17 (d, $J = 8.5$ Hz, 1H), 7.87 (s, 1H), 7.80 (s, 1H), 7.59 (d, J
24 = 1.9 Hz, 1H), 7.30 (d, $J = 10.4$ Hz, 3H), 3.90 (s, 6H), 3.88 (s, 3H). ^{13}C NMR (101 MHz, Methylene
25 Chloride- d_2 : Methanol- $d_4 = 10$: 1) δ 184.48, 153.73, 148.37, 142.54, 137.94, 133.90, 126.73,
26 124.56, 124.45, 124.42, 122.51, 116.67, 115.32, 115.27, 107.20, 106.91, 61.21, 56.77. HRMS:
27 calculated for $\text{C}_{21}\text{H}_{19}\text{BrN}_3\text{O}_4$ $[\text{M}+\text{H}]^+$ 456.0559, found 456.0560. Purity: 99.1% by HPLC ($R_t =$
28 2.14 min).

29
30
31
32
33
34
35
36
37
38
39
40 **(2-(6-(benzyloxy)-1H-indol-3-yl)-1H-imidazol-4-yl)(3,4,5-trimethoxyphenyl)methanone**
41 **(10ao).** obtained as a yellowish solid (21.8 mg, 44.2% from **9ao**). ^1H NMR (400 MHz, Methylene
42 Chloride- d_2) δ 9.54 (s, 1H), 8.21 (d, $J = 8.6$ Hz, 1H), 7.83 (d, $J = 7.0$ Hz, 2H), 7.49 – 7.20 (m, 7H),
43 7.00 – 6.84 (m, 2H), 4.98 (s, 2H), 3.86 (s, 3H), 3.84 (s, 6H). ^{13}C NMR (101 MHz, Methylene
44 Chloride- d_2) δ 156.66, 153.75, 142.52, 137.89, 137.81, 133.88, 129.02, 128.41, 128.12, 124.92,
45 122.11, 120.08, 112.30, 107.17, 96.74, 70.92, 61.17, 56.75. HRMS: calculated for $\text{C}_{28}\text{H}_{26}\text{N}_3\text{O}_5$
46 $[\text{M}+\text{H}]^+$ 484.1872, found 484.1880. Purity: 98.4% by HPLC ($R_t = 2.34$ min).

(2-(6-methoxy-1H-indol-3-yl)-1H-imidazol-4-yl)(3,4,5-trimethoxyphenyl)methanone

(10ap). obtained as a yellowish solid (19.8 mg, 48.3% from **9ap**). ¹H NMR (400 MHz, Methylene Chloride-*d*₂: Methanol-*d*₄ = 10: 1) δ 8.12 (dd, J = 8.7, 0.6 Hz, 1H), 7.79 (d, J = 5.8 Hz, 2H), 7.27 (s, 2H), 6.94 (d, J = 2.2 Hz, 1H), 6.88 (dd, J = 8.8, 2.3 Hz, 1H), 3.91 (s, 6H), 3.87 (s, 3H), 3.83 (s, 3H). ¹³C NMR (101 MHz, Methylene Chloride-*d*₂: Methanol-*d*₄ = 10: 1) δ 184.25, 157.54, 153.75, 149.09, 142.51, 137.98, 133.96, 125.15, 121.60, 119.63, 111.53, 107.14, 106.61, 95.58, 95.52, 61.20, 56.78, 56.06. HRMS: calculated for C₂₂H₂₂N₃O₅ [M+H]⁺ 408.1559, found 408.1567. Purity: 95.0% by HPLC (R_t = 1.89 min).

Methyl 3-(4-(3,4,5-trimethoxybenzoyl)-1H-imidazol-2-yl)-1H-indole-6-carboxylate (10aq).

obtained as a yellowish solid (22.0 mg, 50.5% from **9aq**). ¹H NMR (400 MHz, DMSO-*d*₆) δ 13.21 (s, 1H), 11.98 (s, 1H), 8.52 (d, J = 8.4 Hz, 1H), 8.45 (s, 1H), 8.15 (s, 1H), 8.00 (s, 1H), 7.77 (d, J = 8.4 Hz, 1H), 7.49 (s, 2H), 3.91 (s, 6H), 3.88 (s, 3H), 3.79 (s, 3H). ¹³C NMR (101 MHz, DMSO-*d*₆) δ 182.97, 166.98, 152.62, 141.15, 135.65, 133.24, 129.07, 128.45, 127.98, 127.74, 127.50, 123.27, 120.91, 120.60, 117.93, 113.86, 106.82, 106.36, 60.14, 55.98, 51.84. HRMS: calculated for C₂₃H₂₂N₃O₆ [M+H]⁺ 436.1509, found 436.1508. Purity: 99.7% by HPLC (R_t = 1.98 min).

(2-(7-methyl-1H-indol-3-yl)-1H-imidazol-4-yl)(3,4,5-trimethoxyphenyl)methanone (10ar).

obtained as a yellowish solid (18.7 mg, 47.7% from **9ar**). ¹H NMR (400 MHz, Methylene Chloride-*d*₂: Methanol-*d*₄ = 10: 1) δ 8.09 (dt, J = 7.7, 0.9 Hz, 1H), 7.92 (s, 1H), 7.81 (s, 1H), 7.28 (s, 2H), 7.14 (dd, J = 8.1, 7.1 Hz, 1H), 7.05 (dt, J = 7.2, 1.0 Hz, 1H), 3.90 (s, 6H), 3.88 (s, 3H), 2.51 (s, 3H). ¹³C NMR (101 MHz, Methylene Chloride-*d*₂: Methanol-*d*₄ = 10: 1) δ 184.19, 153.74, 149.12, 142.49, 136.79, 136.65, 133.95, 126.24, 126.08, 124.99, 124.96, 123.86, 121.99, 121.95, 121.75, 118.53, 107.15, 107.08, 107.03, 61.18, 56.76, 16.91. HRMS: calculated for C₂₂H₂₂N₃O₄ [M+H]⁺ 392.1610, found 392.1619. Purity: 99.4% by HPLC (R_t = 1.92 min).

(2-(7-(benzyloxy)-1H-indol-3-yl)-1H-imidazol-4-yl)(3,4,5-trimethoxyphenyl)methanone

(10as). obtained as a yellowish solid (24.6 mg, 50.8% from **9as**). ¹H NMR (400 MHz, Methylene Chloride-*d*₂) δ 9.29 (s, 1H), 7.95 (d, J = 2.9 Hz, 1H), 7.90 (d, J = 8.1 Hz, 1H), 7.84 (s, 1H), 7.54 – 7.47 (m, 2H), 7.44 – 7.33 (m, 3H), 7.30 (s, 2H), 7.15 (t, J = 7.9 Hz, 1H), 6.82 (dd, J = 7.8, 0.7 Hz, 1H), 5.24 (s, 2H), 3.90 (s, 6H), 3.87 (s, 3H). ¹³C NMR (101 MHz, Methylene Chloride-*d*₂) δ 183.55, 153.81, 146.12, 142.59, 137.54, 133.81, 129.15, 128.74, 128.43, 127.78, 126.94, 125.29, 122.36, 114.16, 107.82, 107.07, 104.86, 70.93, 61.17, 56.81. HRMS: calculated for C₂₈H₂₆N₃O₅ [M+H]⁺ 484.1872, found 484.1882. Purity: 99.6% by HPLC (R_t = 2.37 min).

(2-(7-methoxy-1H-indol-3-yl)-1H-imidazol-4-yl)(3,4,5-trimethoxyphenyl)methanone

(10at). obtained as a yellowish solid (16.9 mg, 41.1% from **9at**). ¹H NMR (400 MHz, Methylene Chloride-*d*₂ : Methanol-*d*₄ = 10: 1) δ 7.88 (s, 1H), 7.85 – 7.77 (m, 2H), 7.28 (s, 2H), 7.17 (t, J = 7.9 Hz, 1H), 6.74 (dd, J = 7.9, 0.8 Hz, 1H), 3.98 (s, 3H), 3.91 (s, 6H), 3.88 (s, 3H). ¹³C NMR (101 MHz, Methylene Chloride-*d*₂ : Methanol-*d*₄ = 10: 1) δ 184.15, 153.77, 147.11, 142.55, 133.91, 127.59, 126.64, 125.67, 122.28, 113.43, 107.26, 107.12, 103.42, 61.20, 56.79, 56.01. HRMS: calculated for C₂₂H₂₂N₃O₅ [M+H]⁺ 408.1559, found 408.1560. Purity: 100.0% by HPLC (R_t = 1.90 min).

(2-(5-hydroxy-1H-indol-3-yl)-1H-imidazol-4-yl)(3,4,5-trimethoxyphenyl)methanone

(10au). obtained as a yellowish solid (7.2 mg, 36.5% from **10ak**). ¹H NMR (400 MHz, DMSO-*d*₆) δ 12.88 (d, J = 58.5 Hz, 1H), 11.48 – 10.98 (m, 1H), 8.84 (d, J = 12.5 Hz, 1H), 8.25 (d, J = 2.8 Hz, 1H), 7.89 (d, J = 3.5 Hz, 1H), 7.83 (q, J = 2.0, 1.3 Hz, 1H), 7.24 (dd, J = 8.6, 2.3 Hz, 1H), 7.18 (s, 1H), 6.69 (ddd, J = 11.2, 8.7, 2.5 Hz, 1H), 3.84 (dd, J = 47.9, 6.9 Hz, 9H). HRMS: calculated for C₂₁H₂₀N₃O₅ [M+H]⁺ 394.1403, found 394.1390. Purity: 99.7% by HPLC (R_t = 1.53 min).

(2-(6-hydroxy-1H-indol-3-yl)-1H-imidazol-4-yl)(3,4,5-trimethoxyphenyl)methanone

(10av). obtained as a yellowish solid (8.5 mg, 43.1% from **10ao**). ¹H NMR (400 MHz, Methylene Chloride-*d*₂: Methanol-*d*₄ = 10: 1) δ 7.89 (s, 1H), 7.79 (s, 1H), 7.71 (dd, J = 8.0, 0.9 Hz, 1H), 7.27 (s, 2H), 7.09 (t, J = 7.9 Hz, 1H), 6.70 (dd, J = 7.7, 0.8 Hz, 1H), 3.92 (s, 6H), 3.88 (s, 3H). HRMS: calculated for C₂₁H₂₀N₃O₅ [M+H]⁺ 394.1403, found 394.1418. Purity: 98.4% by HPLC (R_t = 1.59 min).

(2-(1H-indol-4-yl)-1H-imidazol-4-yl)(3,4,5-trimethoxyphenyl)methanone (10bb). obtained

as a yellowish solid (18.8 mg, 49.7% from **9bb**). ¹H NMR (400 MHz, Chloroform-*d*) δ 11.06 (s, 1H), 8.80 (s, 1H), 7.94 (s, 1H), 7.69 (d, J = 7.4 Hz, 1H), 7.47 (dt, J = 8.2, 0.9 Hz, 1H), 7.33 (t, J = 2.9 Hz, 2H), 7.26 (d, J = 1.7 Hz, 1H), 7.20 (t, J = 7.8 Hz, 1H), 3.96 (s, 3H), 3.91 (s, 6H). ¹³C NMR (101 MHz, Chloroform-*d*) δ 183.67, 153.30, 142.36, 136.84, 133.00, 126.16, 125.49, 121.97, 120.82, 119.18, 113.41, 106.78, 102.88, 61.15, 56.45. HRMS: calculated for C₂₁H₂₀N₃O₄ [M+H]⁺ 378.1454, found 378.1457. Purity: 95.5% by HPLC (R_t = 1.78 min).

(2-(1H-indol-5-yl)-1H-imidazol-4-yl)(3,4,5-trimethoxyphenyl)methanone (10bc). obtained

as a yellowish solid (17.2 mg, 45.5% from **9bc**). ¹H NMR (400 MHz, Methylene Chloride-*d*₂) δ 9.34 (s, 1H), 8.28 (d, J = 1.6 Hz, 1H), 7.83 (dd, J = 8.6, 1.7 Hz, 1H), 7.80 (s, 1H), 7.51 (d, J = 8.6 Hz, 1H), 7.31 (dt, J = 2.7, 1.2 Hz, 1H), 7.26 (s, 2H), 6.61 (dt, J = 3.0, 1.3 Hz, 1H), 3.91 (s, 6H), 3.88 (s, 3H). ¹³C NMR (101 MHz, Chloroform-*d*) δ 183.52, 153.35, 142.35, 137.06, 133.13, 128.33, 125.77, 120.90, 120.78, 119.55, 111.83, 106.70, 103.64, 61.15, 56.43. HRMS: calculated for C₂₁H₂₀N₃O₄ [M+H]⁺ 378.1454, found 378.1451. Purity: 95.7% by HPLC (R_t = 1.77 min).

(2-(1H-indol-6-yl)-1H-imidazol-4-yl)(3,4,5-trimethoxyphenyl)methanone (10bd). obtained

as a yellowish solid (16.8 mg, 44.4% from **9bd**). ¹H NMR (400 MHz, Chloroform-*d*) δ 11.02 (s,

1
2
3 1H), 8.77 (s, 1H), 7.95 (s, 1H), 7.79 – 7.65 (m, 1H), 7.49 (d, J = 8.1 Hz, 1H), 7.36 (t, J = 2.8 Hz,
4 1H), 7.32 – 7.16 (m, 4H), 3.97 (s, 3H), 3.92 (s, 6H). ¹³C NMR (101 MHz, Chloroform-*d*) δ 183.29,
5 153.36, 151.90, 142.38, 138.95, 136.83, 132.97, 131.17, 126.23, 125.52, 122.01, 120.72, 119.32,
6 113.51, 106.55, 102.84, 61.16, 56.45. HRMS: calculated for C₂₁H₂₀N₃O₄ [M+H]⁺ 378.1454, found
7 378.1437. Purity: 100.0% by HPLC (R_t = 1.78 min).

14
15
16 **(2-(1H-indol-7-yl)-1H-imidazol-4-yl)(3,4,5-trimethoxyphenyl)methanone (10be)**. obtained
17 as a yellowish solid (18.8 mg, 49.7% from **9be**). ¹H NMR (400 MHz, Chloroform-*d*) δ 8.58 (s,
18 1H), 8.24 (d, J = 7.5 Hz, 1H), 7.93 (d, J = 3.6 Hz, 1H), 7.87 (dd, J = 7.8, 0.8 Hz, 1H), 7.72 (s, 2H),
19 7.60 (t, J = 7.7 Hz, 1H), 7.02 (d, J = 3.7 Hz, 1H), 3.97 (d, J = 0.9 Hz, 9H). ¹³C NMR (101 MHz,
20 Chloroform-*d*) δ 186.04, 153.10, 143.96, 143.25, 142.87, 142.05, **132.31**, 132.01, 128.20, 125.87,
21 124.94, 123.97, 121.35, 120.31, 112.94, 110.91, 108.31, 61.14, 56.49. HRMS: calculated for
22 C₂₁H₂₀N₃O₄ [M+H]⁺ 378.1454, found 378.1469. Purity: 96.5% by HPLC (R_t = 2.43 min).

23
24
25
26
27
28
29
30
31
32
33 **Cell culture and reagents.** Human melanoma carcinoma cell lines A375, M14, and WM164
34 (American Type Culture Collection or ATCC, Manassas, VA, USA) were cultured in Dulbecco's
35 modified Eagle's medium (DMEM) (Corning, Manassas, VA) supplemented with 10% (v/v) fetal
36 bovine serum (FBS) (Atlanta Biologicals, Lawrenceville, GA) and 1% antibiotic/antimycotic
37 mixture (Sigma-Aldrich, St. Louis MO). Murine melanoma B16F10 cells (ATCC, Manassas, VA,
38 USA) were cultured in Minimum essential medium (Invitrogen, Carlsbad, CA), supplemented with
39 5% heat-inactivated Hyclone FBS (Thermo Scientific, Rockford, IL), 1 % antibiotic-antimycotic
40 mixture (Sigma-Aldrich, St. Louis MO), 1% Mem-sodium pyruvate (Invitrogen, Carlsbad, CA),
41 1% Mem-vitamin (Invitrogen, Carlsbad, CA), L-Glutamine (2mM final concentration)
42 (Invitrogen, Carlsbad, CA), and 1% Mem NEAA (Invitrogen, Carlsbad, CA). All cell lines were
43 authenticated by ATCC by short tandem repeat profiling. Cultures were maintained to 80-90%
44
45
46
47
48
49
50
51
52
53
54
55
56
57
58
59
60

1
2
3 confluency at 37°C in a humidified atmosphere containing 5% CO₂. Compounds were dissolved
4
5 in dimethyl sulfoxide (DMSO) (Sigma-Aldrich, St. Louis, MO) to make a stock solution of 20
6
7 mM. Compound solutions were freshly prepared by diluting stocks with cell culture medium
8
9
10 before use.

11
12
13 **Cytotoxicity assay.** A375, M14, and WM-164 were seeded in 96-well plates at a concentration
14
15 of 1,000–5,000 cells per well, depending on the growth rate of the cell line. After overnight
16
17 incubation, the media was replaced and cells were treated with the test compounds at 10
18
19 concentrations ranging from 0.03 nM to 1 μM plus a vehicle control for 72 h in four replicates.
20
21 Following treatment, the MTS reagent (Promega, Madison, WI) was added to the cells and
22
23 incubated in dark at 37°C for at least 1 h. Absorbance at 490 nm was measured using a plate reader
24
25 (DYNEX Technologies, Chantilly VA). Percentages of cell survival versus drug concentrations
26
27 were plotted, and the IC₅₀ (concentration that inhibited cell growth by 50% of untreated control)
28
29 values were obtained by nonlinear regression analysis using GraphPad Prism (GraphPad Software,
30
31 San Diego, CA).
32
33
34
35
36

37 **Protein expression and purification.** The stathmin-like domain of RB3(RB3-SLD) was
38
39 transformed into and over-expressed in *E. coli*. The cells were harvested and resuspended in the
40
41 lysis buffer containing 20 mM Tris-HCl pH 8.0, 1 mM EGTA, 2 mM DTT with the antiprotease
42
43 cocktail and the protein was purified by anion-exchange chromatography and gel filtration
44
45 chromatography. The peak fractions from gel filtration column were concentrated to 10 mg/mL
46
47 and stored at -80 °C⁴⁰⁻⁴². TTL protein was expressed and purified from *E. coli* expression system
48
49 as described in the previous reference⁴³. Briefly, the cells were induced overnight by adding IPTG
50
51 at 25 °C in the LB medium. And the cells were harvested and sonicated in the lysis buffer. The
52
53
54
55
56
57
58
59
60

1
2
3 soluble fraction of the lysate was loaded onto Ni-NTA affinity chromatography and then gel
4
5 filtration chromatography. The final pure sample was concentrated to 20 mg/mL and saved at -80
6
7 °C. The purity of RB3 and TTL were examined by SDS-PAGE. Porcine brain tubulin was supplied
8
9 at 10 mg/mL in G-PEM (General tubulin buffer: 80 mM PIPES pH6.9, 2 mM MgCl₂, 0.5 mM
10
11 EGTA and 1 mM GTP) as a frozen liquid and saved at -80 °C until use.
12
13
14
15

16 **Crystallization and crystal soaking.** Detailed process to making crystals of T2R-TTL was
17
18 according to references ⁴³⁻⁴⁴. In brief, the protein complex containing Tubulin (10 mg/mL), TTL(20
19
20 mg/mL) and RB3 (6 mg/mL) at the molar ratio of 2:1.3:1.2 (Tubulin: RB3: TTL), were incubated
21
22 on ice supplemented with 1 mM AMPPCP, 5 mM tyrosinol and 10 mM DTT, and then
23
24 concentrated to 20 mg/mL at 4 °C. Crystals of T2R-TTL were grown at 20 °C using the sitting-
25
26 drop vapor diffusion method by mixing 1.0 μL protein complex and 1.0 μL crystallization buffer
27
28 containing 6% PEG, 5% glycerol, 0.1M MES, 30 mM CaCl₂, 30 mM MgCl₂, pH 6.7. Initial
29
30 crystals were observed after two days and then the crystal could reach to the final size around a
31
32 length of 200-300 μm within 3-5 days. For the compound soaking to the crystals, the compound
33
34 of ABI-231, **10ab**, **10bb**, were dissolved in DMSO at 10 mM concentration. The crystals were
35
36 soaked with ABI-231, **10ab**, **10bb** (0.1 μL) at 20 °C for 2-24 h, respectively. The crystals were
37
38 quickly dumped into the cryoprotectant (30 mM MgCl₂, 30 mM CaCl₂, 0.1 M MES, pH6.7,
39
40 contained 20% glycerol) and flash frozen in a 100 K liquid nitrogen for data collection.
41
42
43
44
45
46
47

48 **X-Ray data collection and structure determination.** The crystals of the T2R-TTL-ligand
49
50 complexes were mounted in nylon loops and flash-cooled in a cold nitrogen stream at 100K. The
51
52 diffraction data were collected on beamlines BL19U1 at Shanghai Synchrotron Radiation Facility
53
54 (SSRF) in Shanghai, China. Data were initially processed by the HKL2000 program package ⁴⁵.
55
56
57
58
59
60

1
2
3 The previously published T2R-TTL structure (PDB ID: 4I55) as a searching model in the
4 molecular replacement was used to determine the initial phase. The final model was manually built
5 with Coot and all refinements were performed with phenix refine module of Phenix program ⁴⁶.
6
7 The model quality was checked with the PROCHECK program, which shows a good
8 stereochemistry according to the Ramachandran plot.
9
10
11
12
13
14

15 ***In Vitro* Tubulin Polymerization Assay.** Bovine brain tubulin (0.4 mg, >97% pure)
16 (Cytoskeleton, Denver, CO) was mixed with 10 μ M of the test compounds and incubated in 100
17 μ L of general tubulin buffer (80 mM PIPES, 2.0 mM MgCl₂, 0.5 mM EGTA, and 1 mM GTP) at
18 pH 6.9. The absorbance of wavelength at 340 nm was monitored every 1 min for 20 min by the
19 SYNERGY 4 Microplate Reader (Bio-Tek Instruments, Winooski, VT). The spectrophotometer
20 was set at 37 °C for tubulin polymerization.
21
22
23
24
25
26
27
28
29

30 **Fluorescence microscopy.** WM164 cells were seeded and allowed to adhere to glass coverslips
31 in 6 well plates (500,000 cells/well) overnight. Cells were incubated for 18 h with 50 nM of **10ab**
32 or docetaxel. DMSO was added to the cells in equivalent volume as a negative control.
33 Microtubules were visualized with anti- α -tubulin antibody (Thermo Scientific, Rockford, IL) and
34 Alexa Fluor 647 goat anti-mouse IgG (Molecular Probes, Eugene, OR). The coverslips were
35 mounted with Prolong Diamond Antifade mounting media with DAPI (Invitrogen, Eugene, OR)
36 and images acquired with a Zeiss 710 Confocal microscope and Zen imaging software (Zeiss,
37 Thornwood, NY).
38
39
40
41
42
43
44
45
46
47
48
49

50 **Colony forming assay.** A375 cells were plated in replicates of 4 in 6 well plates at a
51 concentration of 500 cells/well in DMEM containing full cell culture media. Seeded cells were
52 then incubated at 37°C overnight to allow cell attachment to the plate bottom. Media was changed
53
54
55
56
57
58
59
60

1
2
3 and cells were treated with the compound or equivalent vehicle (DMSO) control and incubated for
4
5 another week. At the end of this period, cells were fixed with chilled methanol (5 min), stained
6
7 with 0.5% crystal violet solution (4 h), rinsed with sterile water, and air-dried overnight. Images
8
9 were taken and colony area was quantified with ImageJ software (NIH, Bethesda, MD).
10
11
12

13 **Scratch migration assay.** A375 and RPMI7951 cells were seeded in 24 well plates in 4
14
15 replicates at a concentration of 200,000 cells/well and incubated overnight. This concentration
16
17 allowed a confluent monolayer to form in the wells. Using a 200 μ L pipette tip, a straight line was
18
19 scratched through the cell monolayer to remove an area of cells. The plates were then washed
20
21 several times with media to remove any debris and uprooted cells. Cells were treated with 25 nM
22
23 of **10ab**, **10bb** or vehicle control. Images were obtained after 0 h, 12 h, and 24 h with Evos Fl
24
25 Imaging System (LifeTechnologies, Carlsbad, CA). Analysis was performed with ImageJ software
26
27 (NIH, Bethesda, MD).
28
29
30
31
32

33 **Liver microsomes stability assay.** The NADPH regenerating agent solutions A (catalog#:
34
35 451220) and B (catalog#: 451200) and mouse liver microsomes (CD-1, a mixture of male,
36
37 catalog#:452701, and female, catalog#: 452702) were obtained from BD Gentest (Woburn, MA).
38
39 Liver microsomes stability assay was conducted following literature reports ⁴⁷⁻⁴⁸. For each test
40
41 compound, the mouse liver microsomal solution was prepared by adding 0.058 mL of concentrated
42
43 mouse liver microsomes (20 mg/mL protein concentration) to 1.756 mL of 0.1 M potassium
44
45 phosphate buffer (pH 7.4) containing 5 μ L of 0.5 M EDTA to make a 0.6381 mg/mL (protein)
46
47 microsomal solution. Each test compound (2.2 μ L of 10 mM DMSO solution) was added directly
48
49 to 1.79 mL of mouse liver microsomal solution and 90 μ L was transferred to wells in 96-well
50
51 plates (0, 0.25, 0.5, 1, 2, and 4 h time points each in triplicate). The NADPH regenerating agent
52
53 was prepared by mixing 0.113 mL of NADPH regenerating agent Solutions A, 0.023 mL of
54
55
56
57
58
59
60

1
2
3 solution B and 0.315 mL of 0.1 M potassium phosphate buffer (pH 7.4) for each tested compound.
4
5 To each well of the 96-well plate, 22.5 μ L of the NADPH regenerating agent was added to initiate
6
7 the reaction, and the plate was incubated at 37 $^{\circ}$ C for each time point (0, 0.25, 0.5, 1, 2, and 4 h
8
9 time points each in triplicate). The reaction was quenched by adding 225 μ L of cold acetonitrile
10
11 containing warfarin (4 mg/mL) as an internal control to each well. All of the plates were
12
13 centrifuged at 4000 rpm for 20 min and the supernatants (100 μ L) were transferred to another 96-
14
15 well plate for analysis on UPLC–MS (Waters Acquity UPLC linked to Waters Acquity Photodiode
16
17 Array Detector and Waters Acquity Single Quadrupole Mass Detector) on Acquity UPLC BEH
18
19 C18 1.7 mm (2.1x50 mm) column by running 90–5% gradient for water (+0.1% formic acid) and
20
21 acetonitrile (+0.1% formic acid) in 2 minutes. The area under the single ion recording (SIR)
22
23 channel for the test compound divided by the area under the SIR for internal control at 0-time
24
25 concentration was considered as 100% to calculate remaining concentration at each time point.
26
27 The terminal phase rate constant (k_e) was estimated by linear regression of logarithmically
28
29 transformed concentration versus the data, where $k_e = \text{slope} \times (-\ln 10)$. The half-life $t_{1/2}$ was
30
31 calculated as $\ln 2/k_e$. The intrinsic clearance ($CL_{int,app}$) = $(0.693/\text{in vitro } t_{1/2}) \times (1\text{ml incubation}$
32
33 $\text{volume}/0.5\text{ mg of microsomal protein}) \times (45\text{ mg microsomal protein/gram of liver}) \times (55\text{ g of}$
34
35 $\text{liver/kg body weight})$ ⁴⁸⁻⁴⁹.
36
37
38
39
40
41
42

43 ***In Vivo* Antitumor Efficacy of 10bb in the A375 Melanoma Xenograft Model.** All animal
44
45 experiments were performed in accordance with the NIH animal use guidelines and protocol
46
47 approved by the Institutional Animal Care and Use Committee (IACUC) at the University of
48
49 Tennessee Health Science Center (UTHSC, Memphis, TN). We first estimated the acute maximum
50
51 tolerable dose (MTD) for **10bb** formulated in PEG300. By progressively increasing injection doses
52
53 via i.p. route to 6-8 week old female ICR mice (n=2 per group) (Harlan Laboratories, now Evigo
54
55
56
57
58
59
60

1
2
3 Corporation, Denver, CO, USA) the MTD was estimated to be at least 65 mg/kg. To ensure a
4 safety margin during the repeated treatment, we scaled down the dose to 30 mg/kg and 15 mg/kg
5
6 in the animal experiments. Nude mice, 6–8 weeks old, were purchased from Harlan/Evigo. Groups
7
8 were composed of 6-8 mice per group, with an even number of male and female mice. Logarithmic
9
10 growth phase A375 (5×10^7 cells per ml) cells were prepared in phenyl red-free, FBS-free DMEM
11
12 media and mixed at a 1:1 ratio with Matrigel. Tumors were established by injecting 100 μ l of this
13
14 mixture subcutaneously in the dorsal flank of each mouse (2.5×10^6 cells). After 2 weeks, mice
15
16 were randomly divided into control or treatment groups. **10bb** was dissolved in a 1:1 ratio of
17
18 PEG300: PBS solution to produce desired concentrations. 100 μ l of **10bb** solution corresponding
19
20 to 15 or 30 mg/kg doses were administered via i.p. injection once daily for 14 days. The control
21
22 group was given only a vehicle solution of the same preparation and injected at the same frequency.
23
24 Tumor volume was measured three times a week with a caliper and calculated by using the formula
25
26 $a \times b^2 \times 0.5$, where a and b represented the larger and smaller diameters, respectively. Tumor growth
27
28 inhibition (TGI) at the conclusion of the experiments was calculated as $100 - 100 \times ((T - T_0)/(C -$
29
30 $C_0))$, where T, T_0 , C and C_0 are the mean tumor volume for the specific group on the last day of
31
32 treatment, mean tumor volume of the same group on the first day of treatment, mean tumor volume
33
34 for the vehicle control group on the last day of treatment and mean tumor volume for the vehicle
35
36 control group on the first day of treatment, respectively⁵⁰. Animal activity and body weight were
37
38 monitored during the entire experiment period to assess potential acute toxicity. At the end of the
39
40 experiment, mice were sacrificed and the tumors and tissues were dissected out and fixed in 10%
41
42 buffered formalin phosphate solution for more than 1 week before pathology staining analysis.
43
44
45
46
47
48
49
50

51 52 ***In Vivo* Antitumor Efficacy of 10bb in the B16F10 Experimental Lung Metastasis Model.**

53
54 C57BL/6 mice from Charles River Laboratories International, Inc., age 7–8 weeks old, were used
55
56
57
58
59
60

1
2
3 to study the inhibition effect of **10bb** on lung metastasis of melanoma cells. 9-10 mice per group
4
5 were used for the study, with an even number of males and females divided between the two
6
7 groups. B16F10 melanoma cells growing in a logarithmic growth phase were suspended in the
8
9 conditioned media at a density of 1×10^6 per mL. Each mouse was injected with 100 μ L (1×10^5
10
11 cells) via the lateral tail vein. The treatment started on the third day after the inoculation to ensure
12
13 the initiation of metastasis before beginning treatment. **10bb** (30 mg/kg) was formulated as
14
15 described above. All the treatment solutions were kept in the same volume (100 μ L) and
16
17 administered via i.p. injection for 2 weeks, 5 days a week. The vehicle control group was treated
18
19 by i.p. injection with 100 μ L of PEG300 and PBS in a 1:1 ratio. Mice were sacrificed after 15 days
20
21 after the initiation of the experiment, and the lungs were separated, expanded and preserved in
22
23 10% neutral buffered formalin. The number of lung metastasis nodules was recorded. Major organs
24
25 were also preserved in 10% neutral formalin buffer for subsequent examination of potential
26
27 toxicities. Animal activity and body weight were monitored during the entire experiment period to
28
29 assess acute toxicity.
30
31
32
33
34
35

36 **ANCILLARY INFORMATION**

37
38
39 *Supporting Information:* This material is available free of charge via the Internet at
40
41 <http://pubs.acs.org>.
42
43
44

45 Spectral data for synthetic intermediates and ABI-231analogs (PDF).
46
47

48 Molecular formula strings and biological data (CSV).
49
50

51
52 *PDB ID Codes:* 6O61 (ABI-231), 6O5N (**10ab**), 6O5M (**10bb**): Authors will release the atomic
53
54 coordinates upon article publication.
55
56
57
58
59
60

1
2
3 *Corresponding Author:* Wei Li, Department of Pharmaceutical Sciences, University of Tennessee
4 Health Science Center, Memphis, TN 38163, USA. Phone: 901-448-7532, E-Mail: wli@uthsc.edu
5
6

7
8
9 Weimin Li, West China Hospital, Sichuan University, Chengdu, Sichuan 610041, China. Email:
10 weimin003@scu.edu.cn
11
12

13
14 *Present Addresses:* ^ϕ Chemical Biology Program, Memorial Sloan Kettering Cancer Center, New
15 York, NY, 10065, United States; [⊙] UT Southwestern Medical Center, Dallas, TX, 75390, United
16
17 States.
18
19

20
21
22 *Author Contributions:* [†]Q.W., K.E.A., and Y.W. contributed equally.
23
24

25
26 *Acknowledgment:* This work is supported by NIH/NCI grant R01CA148706 to WL and DDM;
27
28 NIH grants 1S10OD010678-01 and 1S10RR026377-01 to WL. Its contents are solely the
29
30 responsibility of the authors and do not necessarily represent the official views of the NIH.
31
32 Additional support from the University of Tennessee College of Pharmacy Drug Discovery Center.
33
34 We thank Dr. Lei Yang at St. Jude Children's Research Hospital for the metabolic stability
35
36 evaluation for new ABI-231 analogs. We also thank Dr. Benoît Gigant (Institute for Integrative
37
38 Biology of the Cell (I2BC), CEA, CNRS, Univ. Paris-Sud, Université Paris-Saclay, France) and
39
40 Dr. Michel O. Steinmetz (Paul Scherrer Institute, Switzerland) for their kindly to providing the
41
42 plasmids of RB3-SLD and TTL. GK and SWW acknowledge the support of American Lebanese
43
44 Syrian Associated Charities (ALSAC). YW and WML acknowledge the support of National
45
46 Major Scientific and Technological Special Project (Significant New Drugs Development,
47
48 2018ZX09201018-021) for raw data collection in X-ray crystallography studies. No NIH fund was
49
50 used to support the contributions from YW and WML, and all intellectual properties related to this
51
52 paper are owned by the University of Tennessee Research Foundation.
53
54
55
56
57
58
59
60

1
2
3 *Abbreviations:* CBSIs, Colchicine binding site inhibitors; MTAs, Microtubule-targeting agents;
4
5 ABC, ATP-binding cassette; TGI, tumor growth inhibition; CA-4, Combretastatin A4; RABI,
6
7 reverse ABI; TMP, trimethoxyphenyl; structure-activity relationship, SAR; P-glycoprotein, P-gp.
8
9

10
11 **Conflict of Interest Disclosure:** Dr. Wei Li is currently serving as a consultant to Veru Inc., who
12
13 licensed the patents covering all compounds reported in this manuscript for commercial
14
15 development. Veru Inc. did not provide any financial support or have any influence on research
16
17 design, data collections, data analyses, or the writing of this manuscript.
18
19
20
21
22
23
24
25
26
27
28
29
30
31
32
33
34
35
36
37
38
39
40
41
42
43
44
45
46
47
48
49
50
51
52
53
54
55
56
57
58
59
60

1
2
3 **REFERENCES**
4
5

- 6
7 1. Mukhtar, E.; Adhami, V. M.; Mukhtar, H., Targeting microtubules by natural agents for
8 cancer therapy. *Mol Cancer Ther* **2014**, *13* (2), 275-284.
9
10
11 2. Jordan, M. A.; Wilson, L., Microtubules as a target for anticancer drugs. *Nat Rev Cancer*
12 **2004**, *4* (4), 253-265.
13
14
15 3. Heald, R.; Nogales, E., Microtubule dynamics. *J Cell Sci* **2002**, *115* (1), 3-4.
16
17
18 4. Kuppens, I. E., Current state of the art of new tubulin inhibitors in the clinic. *Curr Clin*
19 *Pharmacol* **2006**, *1* (1), 57-70.
20
21
22 5. Loong, H. H.; Yeo, W., Microtubule-targeting agents in oncology and therapeutic potential
23 in hepatocellular carcinoma. *OncoTargets Ther* **2014**, *7*, 575-585.
24
25
26 6. McGuire, S., World Cancer Report 2014. Geneva, Switzerland: World Health
27 Organization, International Agency for Research on Cancer, WHO Press, 2015. *Adv Nutr* **2016**, *7*
28 (2), 418-419.
29
30
31 7. Orr, G. A.; Verdier-Pinard, P.; McDaid, H.; Horwitz, S. B., Mechanisms of Taxol
32 resistance related to microtubules. *Oncogene* **2003**, *22* (47), 7280-7295.
33
34
35 8. Kavallaris, M., Microtubules and resistance to tubulin-binding agents. *Nat Rev Cancer*
36 **2010**, *10* (4), 194-204.
37
38
39 9. Kavallaris, M.; Tait, A. S.; Walsh, B. J.; He, L. F.; Horwitz, S. B.; Norris, M. D.; Haber,
40 M., Multiple microtubule alterations are associated with Vinca alkaloid resistance in human
41 leukemia cells. *Cancer Res* **2001**, *61* (15), 5803-5809.
42
43
44 10. Zagouri, F.; Sergentanis, T. N.; Chrysikos, D.; Dimopoulos, M. A.; Bamias, A.,
45 Etoposides in epithelial ovarian, fallopian tube, or primary peritoneal cancer: a systematic review.
46 *OncoTargets Therapy* **2015**, *8*, 2187-2198.
47
48
49
50
51
52
53
54
55
56
57
58
59
60

- 1
2
3 11. Trendowski, M., Recent advances in the development of antineoplastic agents derived from
4 natural products. *Drugs* **2015**, *75* (17), 1993-2016.
5
6
7
8 12. Aseyev, O.; Ribeiro, J. M.; Cardoso, F., Review on the clinical use of eribulin mesylate for
9 the treatment of breast cancer. *Expert Opin Pharmacother* **2016**, *17* (4), 589-600.
10
11
12 13. Ravelli, R. B. G.; Gigant, B.; Curmi, P. A.; Jourdain, I.; Lachkar, S.; Sobel, A.; Knossow,
13 M., Insight into tubulin regulation from a complex with colchicine and a stathmin-like domain.
14
15
16
17 *Nature* **2004**, *428* (6979), 198-202.
18
19
20 14. Finkelstein, Y.; Aks, S. E.; Hutson, J. R.; Juurlink, D. N.; Nguyen, P.; Dubnov-Raz, G.;
21 Pollak, U.; Koren, G.; Bentur, Y., Colchicine poisoning: the dark side of an ancient drug. *Clin*
22
23
24
25 *Toxicol* **2010**, *48* (5), 407-414.
26
27 15. Borisy, G. G.; Taylor, E. W., The mechanism of action of colchicine. Binding of
28 colchicine-3H to cellular protein. *J Cell Biol* **1967**, *34* (2), 525-533.
29
30
31 16. Kanthou, C.; Tozer, G. M., Microtubule depolymerizing vascular disrupting agents: novel
32 therapeutic agents for oncology and other pathologies. *Int J Exp Pathol* **2009**, *90* (3), 284-294.
33
34
35 17. Stengel, C.; Newman, S. P.; Leese, M. P.; Potter, B. V. L.; Reed, M. J.; Purohit, A., Class
36
37
38
39
40
41
42
43
44
45
46
47
48
49
50
51
52
53
54
55
56
57
58
59
60
19. Lu, Y.; Li, C. M.; Wang, Z.; Ross, C. R.; Chen, J.; Dalton, J. T.; Li, W.; Miller, D. D.,
Discovery of 4-substituted methoxybenzoyl-aryl-thiazole as novel anticancer agents: synthesis,
biological evaluation, and structure-activity relationships. *J Med Chem* **2009**, *52* (6), 1701-1711.

- 1
2
3 20. Chen, J. J.; Wang, Z.; Li, C. M.; Lu, Y.; Vaddady, P. K.; Meibohm, B.; Dalton, J. T.; Miller,
4 D. D.; Li, W., Discovery of novel 2-aryl-4-benzoyl-imidazoles targeting the colchicines binding
5 site in tubulin as potential anticancer agents. *J Med Chem* **2010**, *53* (20), 7414-7427.
6
7
8
9
10 21. Chen, J. J.; Li, C. M.; Wang, J.; Ahn, S.; Wang, Z.; Lu, Y.; Dalton, J. T.; Miller, D. D.; Li,
11 W., Synthesis and antiproliferative activity of novel 2-aryl-4-benzoyl-imidazole derivatives
12 targeting tubulin polymerization. *Bioorg Med Chem* **2011**, *19* (16), 4782-4795.
13
14
15
16
17 22. Chen, J. J.; Ahn, S.; Wang, J.; Lu, Y.; Dalton, J. T.; Miller, D. D.; Li, W., Discovery of
18 novel 2-aryl-4-benzoyl-imidazole (ABI-III) analogues targeting tubulin polymerization as
19 antiproliferative agents. *J Med Chem* **2012**, *55* (16), 7285-7289.
20
21
22
23
24 23. Xiao, M.; Ahn, S. J.; Wang, J.; Chen, J. J.; Miller, D. D.; Dalton, J. T.; Li, W., Discovery
25 of 4-aryl-2-benzoyl-imidazoles as tubulin polymerization inhibitor with potent antiproliferative
26 properties. *J Med Chem* **2013**, *56* (8), 3318-3329.
27
28
29
30
31 24. Hwang, D. J.; Wang, J.; Li, W.; Miller, D. D., Structural optimization of indole derivatives
32 acting at colchicine binding site as potential anticancer agents. *ACS Med Chem Lett* **2015**, *6* (9),
33 993-997.
34
35
36
37
38 25. Li, C. M.; Wang, Z.; Lu, Y.; Ahn, S.; Narayanan, R.; Kearbey, J. D.; Parke, D. N.; Li, W.;
39 Miller, D. D.; Dalton, J. T., Biological activity of 4-substituted methoxybenzoyl-aryl-thiazole: an
40 active microtubule inhibitor. *Cancer Res* **2011**, *71* (1), 216-224.
41
42
43
44
45 26. Lu, Y.; Li, C. M.; Wang, Z.; Chen, J. J.; Mohler, M. L.; Li, W.; Dalton, J. T.; Miller, D.
46 D., Design, synthesis, and SAR studies of 4-substituted methoxylbenzoyl-aryl-thiazoles analogues
47 as potent and orally bioavailable anticancer agents. *J Med Chem* **2011**, *54* (13), 4678-4693.
48
49
50
51
52
53
54
55
56
57
58
59
60

- 1
2
3 27. Li, F.; Lu, Y.; Li, W.; Miller, D. D.; Mahato, R. I., Synthesis, formulation and in vitro
4 evaluation of a novel microtubule destabilizer, SMART-100. *J Control Release* **2010**, *143* (1),
5 151-158.
6
7
8
9
10 28. Alves, F. R. D.; Barreiro, E. J.; Fraga, C. A. M., From nature to drug discovery: the indole
11 scaffold as a 'privileged structure'. *Mini-Rev Med Chem* **2009**, *9* (7), 782-793.
12
13
14 29. Chen, J.; Ahn, S.; Wang, J.; Lu, Y.; Dalton, J. T.; Miller, D. D.; Li, W., Discovery of novel
15 2-aryl-4-benzoyl-imidazole (ABI-III) analogues targeting tubulin polymerization as
16 antiproliferative agents. *J Med Chem* **2012**, *55* (16), 7285-7289.
17
18
19
20
21 30. Kashyap, V. K.; Wang, Q.; Setua, S.; Nagesh, P. K. B.; Chauhan, N.; Kumari, S.;
22 Chowdhury, P.; Miller, D. D.; Yallapu, M. M.; Li, W.; Jaggi, M.; Hafeez, B. B.; Chauhan, S. C.,
23 Therapeutic efficacy of a novel betaIII/betaIV-tubulin inhibitor (VERU-111) in pancreatic cancer.
24
25
26
27
28
29
30
31 31. Wang, Q.; Arnst, K. E.; Wang, Y.; Kumar, G.; Ma, D.; Chen, H.; Wu, Z.; Yang, J.; White,
32 S. W.; Miller, D. D.; Li, W., Structural Modification of the 3,4,5-Trimethoxyphenyl Moiety in the
33 Tubulin Inhibitor VERU-111 Leads to Improved Antiproliferative Activities. *J Med Chem* **2018**,
34
35
36
37
38
39
40 32. Fujioka, H.; Murai, K.; Kubo, O.; Ohba, Y.; Kita, Y., One-pot synthesis of imidazolines
41 from aldehydes: detailed study about solvents and substrates. *Tetrahedron* **2007**, *63* (3), 638-643.
42
43
44 33. Briot, A.; Baehr, C.; Brouillard, R.; Wagner, A.; Mioskowski, C., Concise synthesis of
45 dihydrochalcones via palladium-catalyzed coupling of aryl halides and 1-aryl-2-propen-1-ols. *J*
46
47
48
49
50
51 34. Lee, S. H.; Kohn, H., Cyclic disulfide C(8) iminoporfiromycin: nucleophilic activation of
52 a porfiromycin. *J Am Chem Soc* **2004**, *126* (13), 4281-4292.
53
54
55
56
57
58
59
60

- 1
2
3 35. Guinchar, X.; Vallee, Y.; Denis, J. N., Total synthesis of marine sponge bis(indole)
4 alkaloids of the topsentin class. *J Org Chem* **2007**, *72* (10), 3972-3975.
5
6
7
8 36. Hwang, D. J.; Wang, J.; Li, W.; Miller, D. D., Structural Optimization of Indole Derivatives
9 Acting at Colchicine Binding Site as Potential Anticancer Agents. *ACS Med Chem Lett* **2015**, *6*
10 (9), 993-997.
11
12
13
14 37. Banerjee, S.; Arnst, K. E.; Wang, Y. X.; Kumar, G.; Deng, S. S.; Yang, L.; Li, G. B.; Yang,
15 J. B.; White, S. W.; Li, W.; Miller, D. D., Heterocyclic-fused pyrimidines as novel tubulin
16 polymerization inhibitors targeting the colchicine binding site: structural basis and antitumor
17 efficacy. *J Med Chem* **2018**, *61* (4), 1704-1718.
18
19
20
21
22
23 38. Dorleans, A.; Gigant, B.; Ravelli, R. B. G.; Mailliet, P.; Mikol, V.; Knossow, M.,
24 Variations in the colchicine-binding domain provide insight into the structural switch of tubulin.
25 *P Natl Acad Sci USA* **2009**, *106* (33), 13775-13779.
26
27
28
29
30 39. Takeda, M.; Mizokami, A.; Mamiya, K.; Li, Y. Q.; Zhang, J.; Keller, E. T.; Namiki, M.,
31 The establishment of two paclitaxel-resistant prostate cancer cell lines and the mechanisms of
32 paclitaxel resistance with two cell lines. *Prostate* **2007**, *67* (9), 955-967.
33
34
35
36
37 40. Charbaut, E.; Curmi, P. A.; Ozon, S.; Lachkar, S.; Redeker, V.; Sobel, A., Stathmin family
38 proteins display specific molecular and tubulin binding properties. *J Biol Chem* **2001**, *276* (19),
39 16146-16154.
40
41
42
43 41. Dorleans, A.; Gigant, B.; Ravelli, R. B.; Mailliet, P.; Mikol, V.; Knossow, M., Variations
44 in the colchicine-binding domain provide insight into the structural switch of tubulin. *Proc Natl*
45 *Acad Sci U S A* **2009**, *106* (33), 13775-13779.
46
47
48
49
50
51
52
53
54
55
56
57
58
59
60

- 1
2
3 42. Wang, Y.; Zhang, H.; Gigant, B.; Yu, Y.; Wu, Y.; Chen, X.; Lai, Q.; Yang, Z.; Chen, Q.;
4
5 Yang, J., Structures of a diverse set of colchicine binding site inhibitors in complex with tubulin
6
7 provide a rationale for drug discovery. *FEBS J* **2016**, *283* (1), 102-111.
8
9
10 43. Prota, A. E.; Bargsten, K.; Zurwerra, D.; Field, J. J.; Diaz, J. F.; Altmann, K. H.; Steinmetz,
11
12 M. O., Molecular mechanism of action of microtubule-stabilizing anticancer agents. *Science (New*
13
14 *York, N.Y.)* **2013**, *339* (6119), 587-590.
15
16
17 44. Wang, Y.; Yu, Y.; Li, G. B.; Li, S. A.; Wu, C.; Gigant, B.; Qin, W.; Chen, H.; Wu, Y.;
18
19 Chen, Q.; Yang, J., Mechanism of microtubule stabilization by taccalonolide AJ. *Nat Commun*
20
21 **2017**, *8*, 15787.
22
23
24 45. Otwinowski, Z.; Minor, W., Processing of X-ray diffraction data collected in oscillation
25
26 mode. *Method Enzymol* **1997**, *276*, 307-326.
27
28
29 46. Adams, P. D.; Grosse-Kunstleve, R. W.; Hung, L. W.; Ioerger, T. R.; McCoy, A. J.;
30
31 Moriarty, N. W.; Read, R. J.; Sacchettini, J. C.; Sauter, N. K.; Terwilliger, T. C., PHENIX: building
32
33 new software for automated crystallographic structure determination. *Acta Crystallogr D* **2002**,
34
35 *58*, 1948-1954.
36
37
38 47. Mahindroo, N.; Connelly, M. C.; Punchihewa, C.; Yang, L.; Yan, B.; Fujii, N., Amide
39
40 conjugates of ketoprofen and indole as inhibitors of Gli1-mediated transcription in the Hedgehog
41
42 pathway. *Bioorg Med Chem* **2010**, *18* (13), 4801-4811.
43
44
45 48. Di, L.; Kerns, E. H.; Li, S. Q.; Petusky, S. L., High throughput microsomal stability assay
46
47 for insoluble compounds. *Int J Pharm* **2006**, *317* (1), 54-60.
48
49
50 49. Davies, B.; Morris, T., Physiological-parameters in laboratory-animals and humans.
51
52 *Pharm Res* **1993**, *10* (7), 1093-1095.
53
54
55
56
57
58
59
60

- 1
2
3 50. Wang, J.; Chen, J.; Miller, D. D.; Li, W., Synergistic combination of novel tubulin inhibitor
4
5 ABI-274 and vemurafenib overcome vemurafenib acquired resistance in BRAFV600E melanoma.
6
7
8 *Mol Cancer Ther* **2014**, *13* (1), 16-26.
9
10
11
12
13
14
15
16
17
18
19
20
21
22
23
24
25
26
27
28
29
30
31
32
33
34
35
36
37
38
39
40
41
42
43
44
45
46
47
48
49
50
51
52
53
54
55
56
57
58
59
60

Table of Contents Graph

